Isotopic Constraints on the Depositional Environment and Paleo-Redox Conditions of the Greater McArthur Basin, Northern Territory

Thesis submitted in accordance with the requirements of the University of Adelaide for an Honours Degree in Geology

Maxwell Morrison Bullen

November 2017

THE UNIVERSITY of ADELAIDE

ISOTOPIC AND TRACE ELEMENT CONSTRAINTS ON THE PALEO-DEPOSITIONAL ENVIRONMENT AND REDOX HISTORY OF THE GREATER MCARTHUR BASIN, NORTHERN TERRITORY

RUNNING TITLE

Paleo-Depositional Environment and Redox history of the Greater McArthur Basin

ABSTRACT

The Limbunya Package of the Greater McArthur Basin, Northern Territory, hosts the oldest known hydrocarbon reservoirs. Despite the prospective nature of the Fraynes Formation (ca. 1638 Ma), the depositional environment and redox conditions for these organic-rich sediments and the associated carbonates is not well understood. Utilising high resolution stable and radiogenic isotope proxy records ($\delta^{13}C$, $^{87}Sr/^{86}Sr$ and $^{143}Nd/^{144}Nd$), we show that basin restriction was prevalent during deposition of the Fraynes Formation. As basin restriction has been suggested for the correlative Barney Creek Formation, we argue that this event affected the entire Greater McArthur Basin. The $\delta^{13}C$ and $^{87}Sr/^{86}Sr$ isotopic signatures measured in this study (Manbulloo S1 core) are compared to corresponding stratigraphic units from the central McArthur Basin (LV09001 core). The results show evidence for coherent basin-wide C and Sr isotopic patterns that in turn could be used for the chemostratigraphy purposes during the deposition of the organic rich shales (Fraynes and Barney Creek Formations) and the overlying Reward dolomite sequences. Differences in $\delta^{13}C$ isotope signal in the underlying Campbell Springs Dolomite (Teena Dolomite equivalent) are proposed to be related either to differences in the C isotope composition of local DIC pools at these two paleo-locations (i.e., LV09001 and Manbulloo sites), or the isotopically lighter $\delta^{13}C$ signal in the latter core could reflect deeper depth of the deposition for dolomite at this site. Linking redox-sensitive trace element enrichments with total organic carbon data indicates that the water column was anoxic to euxinic during the deposition of the Fraynes Formation, with episodes of euxinia driven by the relatively high input of organic matter. Overall, knowledge gained here, particularly in regard to the links between paleo-depositional environments, redox conditions, and the occurrences of organic-rich shales, can be applied to other Precambrian frontier basins.

KEYWORDS

Greater McArthur Basin, Paleoproterozoic, C-Sr-Nd Isotopes, Depositional Environment, Redox, Chemostratigraphy

TABLE OF CONTENTS

LIST OF FIGURES

INTRODUCTION

The demand and use of hydrocarbons as an energy source is at a historic high, and this rate is continuing to grow at a rate of ca. 10% p.a. (Olah & Prakash, 2017). These rising energy demands have driven research into discovering and exploiting what was previously recognised as uneconomical source rock, most notably from the increased use of fracking in unconventional shale reservoirs in the last decade (Stephenson, 2015). The intracratonic Greater McArthur Basin of northern Australia is of interest for further exploration because of (i) its large economic potential, hosting high grade mineralisation and some of the world's oldest proven hydrocarbons (Ahmad, Dunster, & Munson, 2013; Munson, 2016; Revie & Edgoose 2015), and also (ii) for its unique sedimentary record that provides a 'window' into the mid-Proterozoic evolution of the Earth's surface environment and the oceans (Shen, Canfield, & Knoll, 2002).

The Greater McArthur Basin comprises of 5 lithologically distinct depositional packages (Rawlings, 1999), with the Mesoproterozoic Wilton package (ca. 1490-1325 Ma) currently attracting intense interest due to the unconventional hydrocarbon potential of the organic rich Kyalla and Velkerri Formations (Close et al., 2017; Cox et al., 2016; Revie & Edgoose, 2015). However, the Paleoproterozoic carbonate-dominated Glyde package (1640-1600 Ma) also contains potentially exploitable hydrocarbon resources, with the Barney Creek Formation being recognised for its hydrocarbon source and unconventional reservoir potential (Crick, Boreham, Cook, & Powell, 1988; Rodrigues et al., 2015).

Geochemical data and strontium isotope ($^{87}Sr/^{86}Sr$) constraints from Giuliano (2016) and Johnston et al. (2008) show that during the deposition of the Barney Creek Formation (ca. 1640 Ma), the McArthur Basin underwent a partial/full restrictive event,

where interaction with the global ocean was inhibited. This event, along with previous research suggesting the McArthur Basin water column was anoxic (Johnston et al., 2008), potentially allowing the onset of free sulphide (euxinic) bottom waters in a stratified water column, analogous to the modern day Black Sea (Fry et al., 1991; German, Holliday, & Elderfield, 1991).

Because of the antiquity of these Palaeoproterozoic source rock, studies focusing on the generation and preservation of organic material over long geological time periods is critical in understanding the potential of such frontier basins both locally and globally. This requires the proper interpretation of the paleo-depositional environment and proxy-based reconstruction of the past changes in the ocean redox structure to fully understand the potential of Precambrian sedimentary basins.

This study will investigate the geochemical properties of the Limbunya Package (Glyde Package equivalent) in order to further understand the conditions present during the deposition of organic rich shales (i.e. Fraynes Formation, presumably an equivalent of the Barney Creek Formation), and the associated carbonate (dolomite) sequences. By linking the isotopic ratios of carbon, strontium and neodymium ($\delta^{13}C$, $^{87}Sr/^{86}Sr$ and εNd) with major and trace elemental abundances, inferences regarding the relative source of continental and marine input into the basin are able to be made, further constraining the paleo-depositional environment as well as the chemical and redox stratification of the basin. Isotopic Tracer, coupled with with organic carbon data (TOC) and paleo-redox proxies, provides evidence for conditions that led to transient euxinia.

Systematic trends in the isotopic signatures of C and Sr are compared to previous studies to determine whether the Greater McArthur Basin has basin wide isotopic patterns that could be used for chemostratigraphy. Alternatively, if there is spatial

variation within the acquired isotope trends, then smaller sub-basins potentially developed individual signatures due to localised effects, and potential contributing factors are briefly discussed.

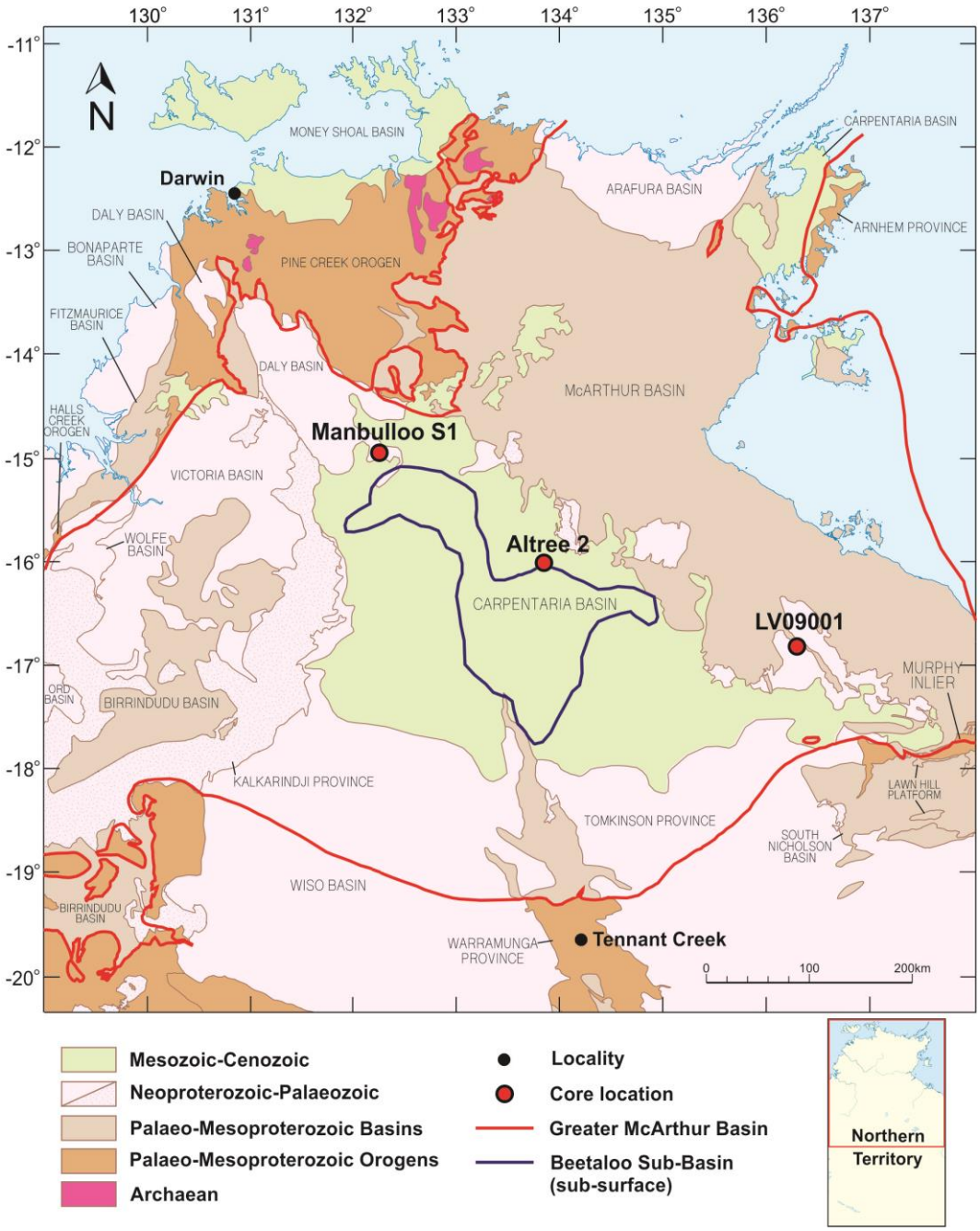

Figure 1: **Geological map of the Northern Territory, showing all major basins and outlining the known extent of the Greater McArthur Basin (Close, 2015) and the Beetaloo Basin (Revie, 2016). The core that underwent geochemical analysis in the study (Manbulloo S1) will be compared with LV09001, which lies ca. 500km to the SE. Map adapted from the Northern Territory Geological Survey (NTGS) Strike database.**

GEOLOGICAL SETTING

The McArthur Basin contains extensive sedimentary packages up to 10 km thick, ranging in age from Paleoproterozoic to Neoproterozoic. The five lithologically distinct packages, as described by Rawlings (1999), are separated by regional unconformities (Ahmad et al., 2013) associated with inversion events (Betts et al., 2016). Previous work within other coeval basins have discovered that the sedimentary succussions from Rawlings (1999) have stratigraphic correlations with the Birrindudu Basin and Tomkinson Province, with the extent of the entire sedimentary sequence referred to as the Greater McArthur Basin (Figure 1; Close, 2014). The intracratonic sedimentary superbasin formed by lithospheric tilting and transpressional rifting, casued by subduction and magmatic arc processes in Central Austalia (Scott et al., 2000). The low oxygen conditions in the coeval ocean-atmosphere system allowed for organic rich black shales to develop, and, despite its antiquity, the basin has experienced a low level of post depositional deformation, which has allowed for the preservation of these hydrocarbon reservoirs (Fennel, Follows, & Falkowski, 2005).

The Limbunya Group consists of mixed carbonate (dolomite) and siliciclastic sequences, reflecting variable conditions of shallow-marine to moderately-deep depositional environments which allowed the formation of extensive stromatolitic carbonate platforms and organic rich shales. The targeted study area within the group is the organic rich Fraynes Formation (Barney Creek Formation equivalent) and the over and underlying dolomitic units. The Fraynes Formation is a laminated dolomitic siltstone with organic rich black shale intervals, with a higher proportion of carbonate up section. U-Pb dating of detrital zircons give a maximum depositional age of 1638 ± 9 Ma (Ahmad & Dunster, 2013). The Fraynes Formation conformably overlies the

Campbell Springs Dolomite, which is mainly a stromatolitic carbonate unit with rare sandstone formed in a shallow marine (possibly tidal) setting. The Reward Dolomite conformably overlies the Fraynes Formation, and consists of mainly dolostone and dolomitic sandstone, and show evidence of evaporates. From this, a shallow lagoon or evaporative shallow marine style of depositional has been proposed (Ahmad & Dunster, 2013). The proposed changes in depositional environment throughout the Limbunya Group stems from sea level change and basin subsidence caused by tectonic processes in central Australia (Schmid, 2015; Scott et al., 2000).

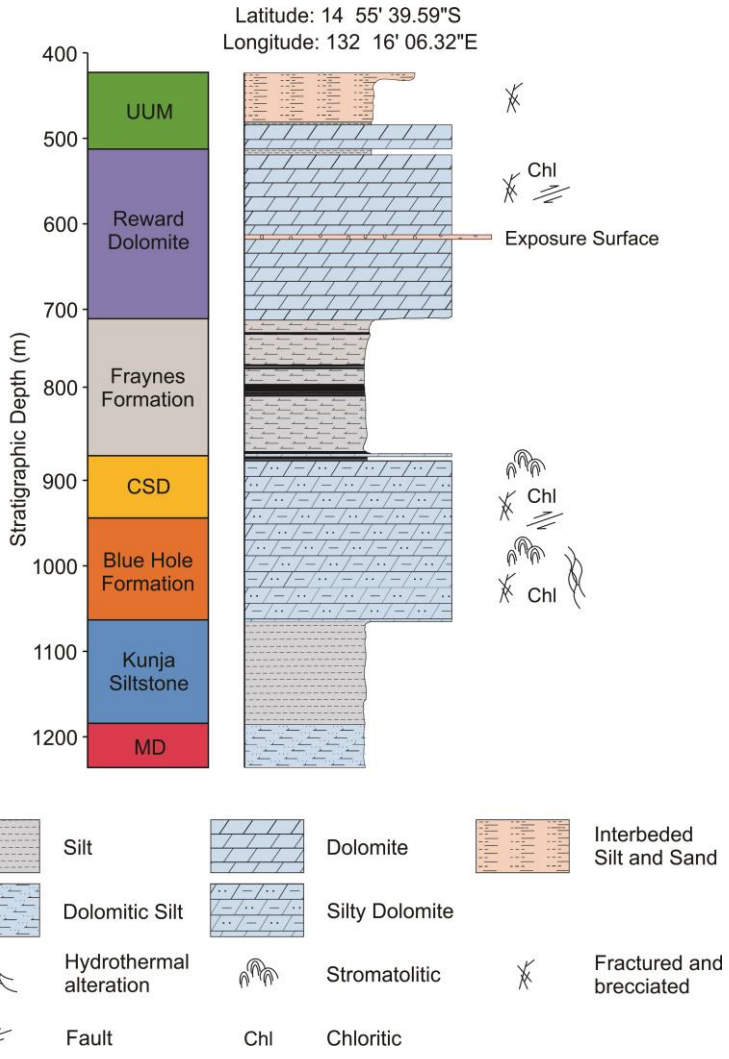

Figure 2: Stratigraphic log of the Manbulloo S1 core, which is the reference core for this study. Stratigraphic abbreviations are as follows: UUM = Undifferentiated Upper McArthur, CSD = Campbell Springs Dolomite, MD = Mallahbah Dolostone.

METHODS

Selection and sampling of drill core

The Manbulloo S1 core, which forms the basis for this study, shows no evidence of large scale alteration, and contains a complete and undisturbed record of the major lithological formations relevant to this study (Figure 2). A total of 215 samples from Manbulloo S1 core were taken from the NTGS core facility in Darwin, and were collected with a resolution of between 3-10 meters, although this was increased to 20 cm intervals in organic rich zones. Variation of resolution was dependent on key lithological boundaries, and proximity to any obvious diagenetic alteration.

TOC and elemental concentration for black shales

Twenty samples taken from the three black shale rich intervals were crushed into a fine power using a tungsten carbide mill and analysed for trace element concentration and Total Organic Carbon (TOC) content. TOC data was collected by measuring the pressure created from the dissolution of ca. 200 mg of rock powder in a solution of 4 M HCl/3% $FeCl_2$ (5 mL), following the method from Sherrod et al. (2002). The TOC was then calculated by measuring the total carbon content within the sample using a Perkin Elmer CHNS/O Elemental Analyser, and subtracting the inorganic carbon fraction from this value. Trace elemental concentration analyses were also taken out on the 20 selected black shale fractions. These were measured using an Agilent 7500 Series ICP-MS with Octopole Reaction System, and achieved on a total digest (Hydrofluoric and Nitric acid). Further analysis of hydrocarbon potential was undertaken on a Weatherford Instruments SRA™ instrument at the University of Adelaide.

$\delta^{13}C$ isotope analysis

A selection of 144 carbonate-rich samples were mirco-drilled along bedding planes, and the rock powder was precisely weighed (ca. 0.5-1 mg) and placed into 1 mL glass septa vials. The vials were purged with helium, and phosphoric acid (ca. 10 drops, 1M) was added. The ratio of the isotopic composition from the resultant gas (CO_2) was measured using a Dual Inlet Isotope Ratio Mass Spectrometer (DI-IRMS) at the University of Adelaide. Of the 144 samples that were run, a total of 14 were repeated and the results from these runs displayed a high reproducibility. The standards used were ANU P3, UAC-1 and CO-8, and the carbonate-associated C isotope ratios expressed are relative to Pee Dee Belemnite (PDB) using the following equation:

$$\delta^{13}C\ (‰) = [(^{13}C/^{12}C_{SAMPLE})/(^{13}C/^{12}C_{STANDARD})\text{-}1] \times 1000$$

$^{87}Sr/^{86}Sr$ isotope analysis

A selection of 32 carbonate-rich samples were mirco-drilled along bedding planes, and the rock powder (ca. 0.5 mg) was washed with ammonium acetate (1.5 mL, 1 M) to remove any loosely bound cations (Bailey, McArthur, Prince, & Thirlwall, 1999). The resulting powder was washed and dried, and the leached with dilute ammonium acetate (2 x 1.5 ml, 10% w/w). The use of a weak acid minimizes the partial dissolution of any clays within the sample (Bailey et al., 1999; Halverson & Hubert-Théou, 2015). The original sample was reconcentrated using high purity nitric acid (3.5 M) and the strontium was separated using ion chromatography in polyprep columns containing Eichrom Sr resin SPS (extended method in Appendix B). The purified Sr fraction (ca. 800 ng of Sr) was loaded onto outgassed rhenium filaments, and the carbonate-associated $^{87}Sr/^{86}Sr$ ratio was measured using an Isotopx Phoenix Thermal

Ionisation Mass Spectrometer (TIMS), operating in double collector dynamic measurement mode. The reproducibility at two standard error was better than 0.000005. Standards used throughout this procedure were JDO-1 and SRM 987.

Samarium and neodymium isotopic analysis

A total of 10 silt-rich intervals covering a majority of the core length were taken for Sm/Nd isotopic analysis. Samples were mircodrilled along bedding planes, and the rock powder (ca. 0.067 g) combined with a mixed spike ($^{147}Sm +^{150}Nd$, ca. 0.45 g) was dissolved in a solution of nitric acid (2 mL, 7M) and hydrofluoric acid (4 mL, 48 wt.%). The sample was then left at 140°C overnight and evaporated and reconcentrated using hydrochloric acid (6 mL, 6 M). Using ion chromatography in polyprep columns containing AG 50W-X8 200-400 mesh resin, the rare earth element fraction was concentrated. The subsequent isolation of both Sm and Nd was carried out in quartz glass columns using Eichrom Ln ion exchange resin. The purified Sm and Nd fractions were loaded onto outgassed rhenium filaments and the analysis was carried out on an Isotopx Pheonix TIMS. Machine fractionation was corrected for through normalisations to a $^{146}Nd/^{144}Nd$ value of 0.721903. The error was consistently lower than 2se = 0.000006. The standard used in this procedure was SCo-1. For a full, detailed methodology and specifications used in the Sm/Nd experimental method, including TIMS mode of function and Nd model assumptions, see Appendix B.

Trace element analysis for carbonates

Carbonate leachates prepared for $^{87}Sr/^{86}Sr$ ratio analysis were also measured for their elemental composition. A fraction of the leachate was diluted with nitric acid (2%)

into aliquots of ca. 1:2000 and ca. 1:100,000 dilutions. These solutions were used to determine elemental concentrations using an Agilent 8900x (QQQ) Inductively Coupled Plasma Mass Spectrometer (ICP-MS). An internal standard (indium) was mixed with the samples to compensate for any potential matrix effects. A calibration curve was established (5 samples, 0-500 ppb) and six blanks were used throughout the sampling. Plasma conditions are shown in extended methods, Appendix B. The standard used was JDO-1.

Cerium anomalies (Ce*), the deviation of the concentration of Ce relative to the Lanthanum (La) and Praseodymium (Pr), were calculated from this trace element data using the following equation from Bau and Dulski (1996):

$$Ce^*_{SN} = Ce_{SN} / \sqrt{La_{SN} \times Pr_{SN}}$$

Where SN denotes that the elemental concentration has been normalised to the Post Archean Australian Shale (PAAS) composite of Nance and Taylor (1976). Praseodymium anomalies (Pr*) are calculated using the same of criteria, where the enrichment is normalised to the neighbouring lanthanides, as shown in the equation from Bau and Dulski (1996):

$$Pr^*_{SN} = Pr_{SN} / \sqrt{Ce_{SN} \times Nd_{SN}}$$

RESULTS

TOC and elemental concentration on black shale fraction

The TOC content for 20 black shale samples ranged from 0.1 to 8.1%, with the highest average TOC content located within the upper Fraynes Formation (Figure 3a). There is an observed covariance in TOC content and the redox sensitive elemental ratios of Mo/Al and U/Al between 0.5 and ca. 4% TOC (Figure 3a and b), and lie along the

same trend observed in Mesoproterozoic black shales of the McArthur Basin (Cox et al., 2016). The Ce anomalies in these dolomitic black shales were exclusively negative for all samples measured.

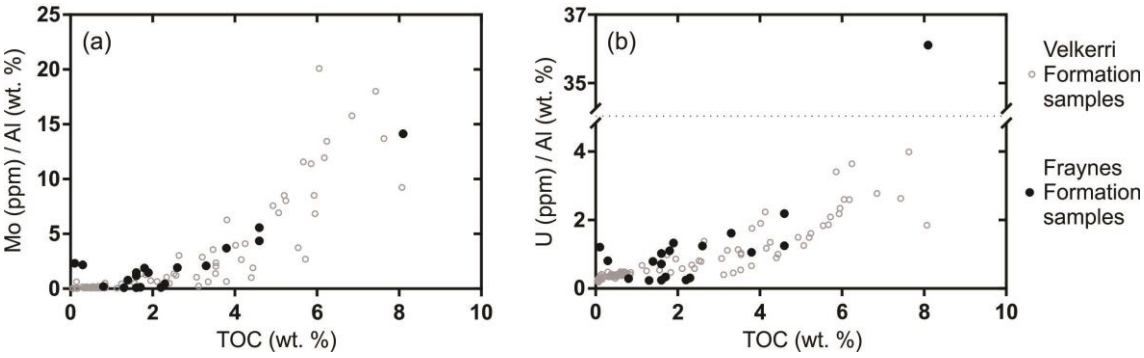

Figure 3: (a and b) Trace element enrichment with respect to TOC. Both molybdenum and uranium have similar trends, showing a covariance with TOC from 0.5 to ca. 4%. The relationship breaks down outside of this range. The elemental concentrations measured were normalised to Al to correct for any detrital component present within the sample (Tribovillard et al., 2006). Data is depicted with results of the Velkerri Shale from the Altree 2 core (Cox et al., 2016).

Organic matter maturity proxies (T_{max}) reveal that mid and upper Fraynes Formation have been heated to within the oil window, samples from the lower Fraynes Formation are overmature (Figure 4b). Free hydrocarbons (S1 –Figure 4c) and residual kerogen (S2 –Figure 4d) all decrease down section. For a full data set of trace element concentrations and hydrocarbon properties, see Appendix A.

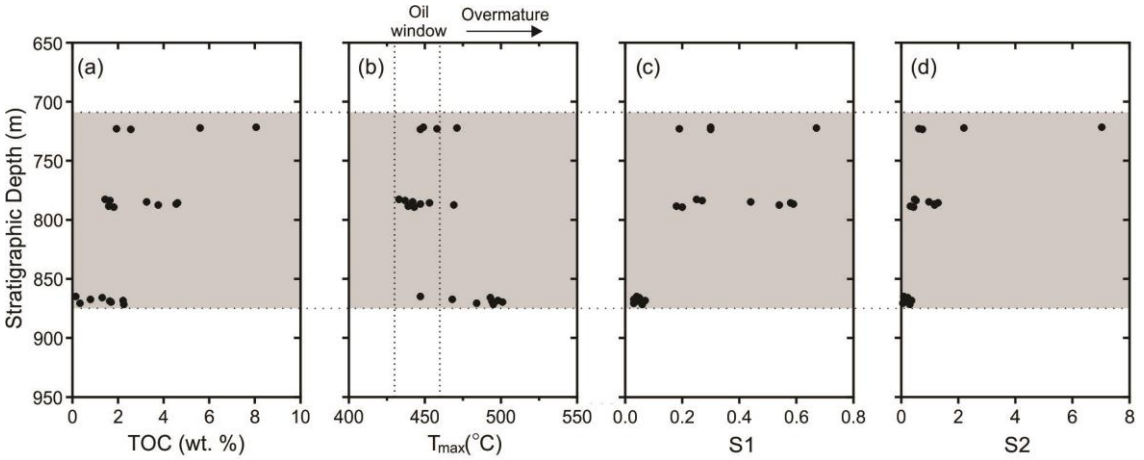

Figure 4: The change of hydrocarbon properties as a function of stratigraphic depth. a) TOC. b) T_{max} –proxy for thermal maturity. c) S1 – measure of free hydrocarbons. d) S2 – residual kerogen. All three black shale layers are deposited within the Fraynes Formation.

$\delta^{13}C$ isotopes

For $\delta^{13}C$ isotope analysis, 144 samples were chosen to give a resolution of ca. 2 m, with higher resolution measured across key lithological boundaries (Reward/Fraynes and Fraynes/Campbell Springs). The spread of $\delta^{13}C$ values within the core was between -3.0‰ and +1.0‰ (Figure 5a). The $\delta^{13}C$ signal is predominantly negative from 1192.5 m -721.1 m, and there is an up-section shift towards more positive values starting within the upper Fraynes Formation. Positive values are observed throughout the rest of the core, except for an extreme negative value of -2.85‰ at 613.9 m belonging to what is interpreted to be an exposure surface. This strong stratigraphic trend in $\delta^{13}C$ values is independent of lithology, as dolomitic members plot in both of the two major positive and negative bands, and the organic rich dolomitic silts of the Fraynes Formation have both negative and positive $\delta^{13}C$ compositions.

$^{87}Sr/^{86}Sr$ isotopes

A total of 32 carbonate rich samples were selected and analysed for their $^{87}Sr/^{86}Sr$ ratio. These values varied from 0.0705161 (2se = 0.000003) to 0.721634 (2se =0.000007) with a mean of 0.709482 (Figure 5b). The variation within the core was paired alongside relevant lithological units, and the mean value of the Fraynes Formation was 0.719919 compared to 0.708524 for all samples of dolomitic composition. The exception is a more radiogenic $^{87}Sr/^{86}Sr$ ratio measured in the lower Blue Hole Formation. The lowest $^{87}Sr/^{86}Sr$ values measured in the dolomitic units (Reward, Campbell Springs, Blue Hole Formations) are consistent with what is considered to be the late Paleo-Proterozoic marine Sr isotope compositions of ca. 0.705-0.707 (Kuznetsov et al., 2010; Veizer & Compston, 1976).

Sm/Nd isotopes

Sm/Nd isotopic ratios were undertaken on 10 shale rich samples representative of all major lithological units, with a resolution of ca. 80 m. The $^{143}Nd/^{144}Nd$ ratios range from 0.510866 and 0.512145, and the initial $^{147}Sm/^{144}Nd$ ratios range from 0.0685-1.848 with an average of 0.1133. The $\varepsilon_{Nd(t)}$ value was between -10.26 and -3.93 (Figure 5c), with an anomalous sample with a highly evolved $\varepsilon_{Nd(t)}$ value of -26.54 at 734.9 m. This single sample is considered an outlier and is omitted from interpretation.

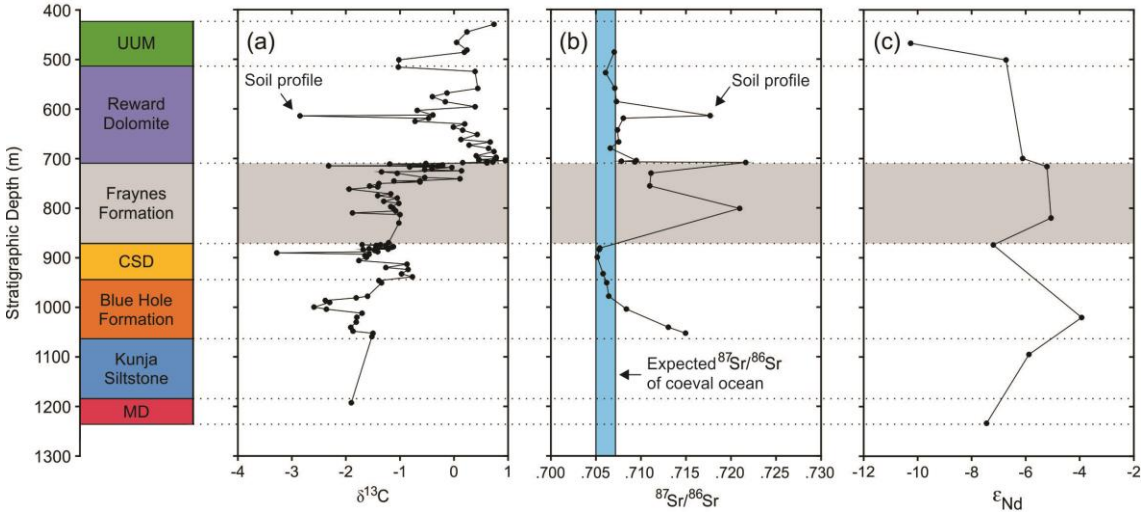

Figure 5: Isotopic data gathered from Manbulloo S1 versus stratigraphic depth. (a) Carbonate-associated $\delta^{13}C$ data showing that the overall trend to more positive values up section, with a relatively sudden shift from -1 to 1‰ occurring in the upper Fraynes Formation. (b) Carbonate-associated $^{87}Sr/^{86}Sr$ ratio, outlining more radiogenic values occurring during the Fraynes Formation. The blue bar represents the $^{87}Sr/^{86}Sr$ ratio range of seawater during the time of deposition (Kuznetsov et al., 2010; Veizer & Compston, 1976). (c) Variation in $\varepsilon_{Nd(t)}$values, showing that there is no significant siliciclastic provenance change occurring during deposition. Stratigraphic abbreviations are as follows: UUM = Undifferentiated Upper McArthur, CSD = Campbell Springs Dolomite, MD = Mallahbah Dolostone.

Major and trace element analysis of carbonate rich members

The 32 carbonate samples measured for their elemental concentrations are illustrated in Figure 6, and show that incompatible elements (Al and K), which are enriched in continental crust, were also enriched during the deposition of the Fraynes Formation and the lower Blue Hole Formation. Iron concentrations show no systematic

change with lithology, and Mn showed a depletion in concentration throughout the Fraynes Formation. The exposure surface at 613.9 m has anomalous values in most elements, with an obvious enrichment in Al, K and Sr, and a depletion in Mn and Fe. The Ce* data showed a small positive anomaly with a maximum of 1.13, while negative values are persistent through the Fraynes Formation with a minimum of 0.93. A full table of all element concentrations measured can be found in Appendix A.

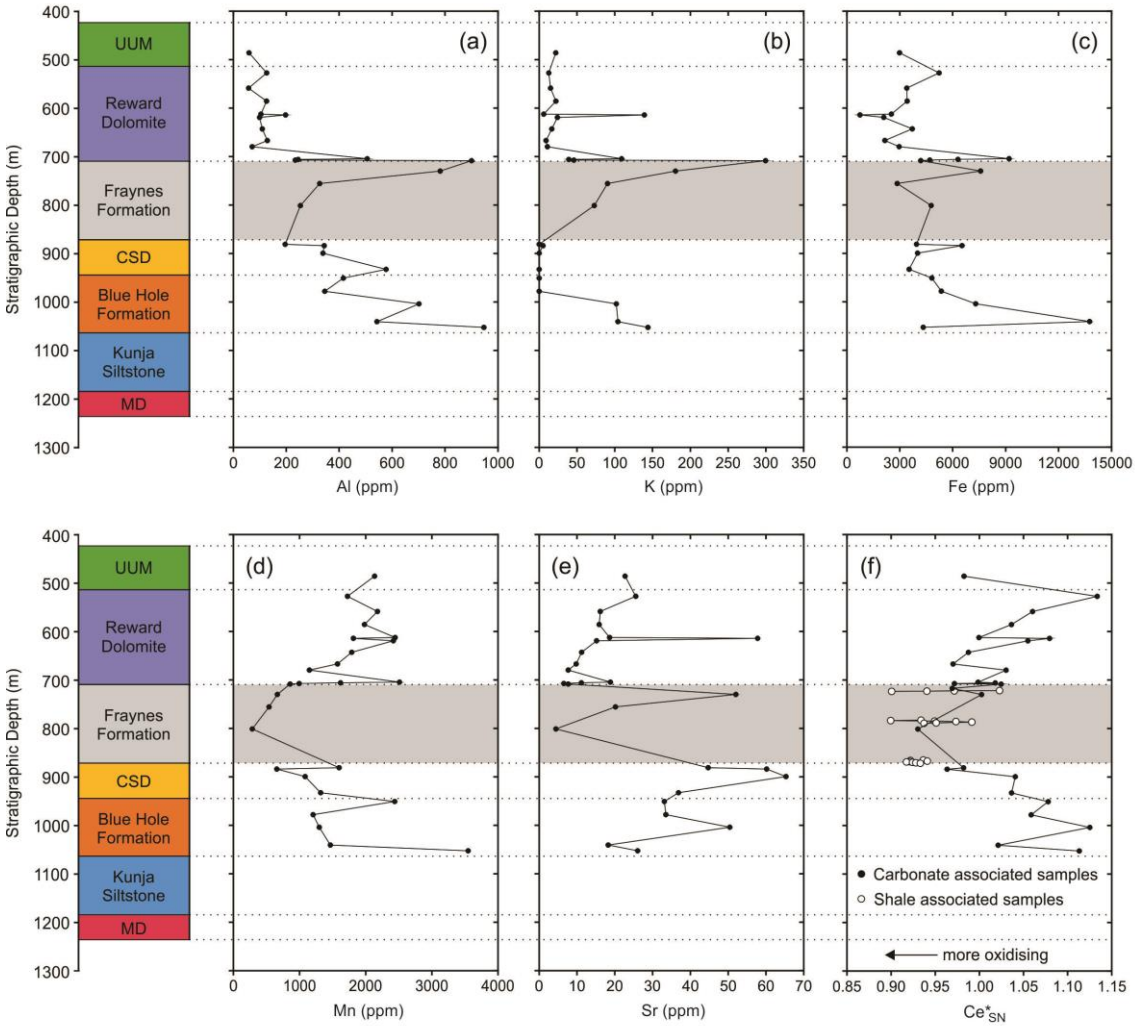

Figure 6: Stratigraphic variation in redox sensitive, major and trace element concentrations. (a) Aluminium. (b) Potassium. (c) Iron. (d) Manganese. (e) Strontium. (f) Cerium anomaly calculated as $Ce^*_{SN} = Ce_{SN}/[\sqrt{La_{SN} \times Pr_{SN}}]$ where SN refers to shale normalisation using values for PAAS from Nance amd Taylor (1976). Stratigraphic abbreviations are as follows: UUM = Undifferentiated Upper McArthur, CSD = Campbell Springs Dolomite, MD = Mallahbah Dolostone.

DISCUSSION

Diagenesis and clay contamination effects on the primary isotope signals

The carbonate-associated $^{87}Sr/^{86}Sr$ ratios are significantly higher in samples from Fraynes Formation compared to the remaining data set. While values directly above and below the Fraynes Formation conform to the marine $^{87}Sr/^{86}Sr$ ratio of 0.0705-0.707 (Kuznetsov et al., 2010), the more radiogenic values measured suggest a greater continental contribution to the $^{87}Sr/^{86}Sr$ ratios in Fraynes Formation samples. A cross plot of Al concentration vs $^{87}Sr/^{86}Sr$ reveals that Fraynes Formation samples with an elevated $^{87}Sr/^{86}Sr$ ratio also have elevated Al concentrations (Figure 7a). Although the rock powder was washed with ammonium acetate, and carefully leached with weak acetic acid, it was determined that these high values are likely due to the dissolution of clay particles (Bailey et al., 1999), and do not represent a primary seawater signature. To eliminate samples impacted by the leaching of radiogenic Sr from clays, only samples with Al concentrations of less than 2000 ppm are considered in the further discussion, due to their presumably least affected $^{87}Sr/^{86}Sr$ signatures by clay contamination.

Possible diagenetic alteration of bulk carbonates by meteoric waters was assessed by plotting the elemental ratio of Sr/Mn against the $^{87}Sr/^{86}Sr$ of studied carbonates, as shown in Figure 7b. This is based on the diagenetic trends noted in Banner and Hanson (1990). Overall, these associations show that there is not any obvious diagenetic influence on $^{87}Sr/^{86}Sr$ ratios, other than in the samples with highly radiogenic Sr and elevated Al (see open squares in Figure 7), which were already removed due to the above-mentioned effects of the dissolution of clay particles in the leachate.

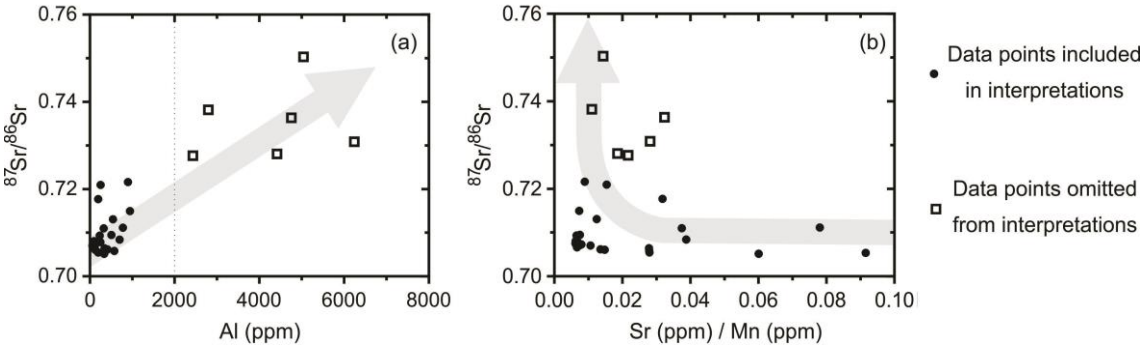

Figure 7: Cross plot of elemental concentration and radiogenic strontium values from the Manbulloo S1 core. a) Aluminium component of samples vs the $^{87}Sr/^{86}Sr$ ratio. The grey arrow indicates increased clay contamination (Bailey et al., 1999). b) $^{87}Sr/^{86}Sr$ vs Sr/Mn concentration. The grey arrow indicates the alteration trend during any mineral-water interaction upon meteoric diagenesis (Banner & Hanson, 1990). General trends showed that diagenesis did not have a great effect on samples, although all data points that had an Al concentration above 2000 ppm were omitted from this study, due to clay contamination.

Paleoredox proxies

To further constrain the redox structure of the water column in the Greater McArthur Basin, this study utilised selected redox sensitive elements including Molybdenum (Mo), Uranium (U), and Cerium (Ce). Molybdenum generally occurs in seawater as the molybdate anion (MoO_4^{-2}), and is the most abundant transition metal in modern ocean (Collier, 1985). Mo is commonly used as a redox proxy as it displays little affinity for detrital minerals, but forms complexes with organic molecules and H_2S under reducing conditions (Tribovillard, Algeo, Lyons, & Riboulleau, 2006). As shown by Scott and Lyons (2012), Mo concentrations in black shales are much higher than average crustal levels, and have a strong correlation with TOC. Under euxinic conditions, Mo can react with both organic matter and H_2S, and is consequently partitioned from the water column at higher rates under sulfidic conditions. Because of this, Mo enrichment and TOC content show a linear covariance under anoxic but non-sulfidic conditions, and exhibit a much stronger non-linear covariance in euxinic

environments, where sinks for Mo include both organic matter and sulphide phases (Cox et al., 2016; Scott & Lyons, 2012).

Uranium in seawater under oxidising conditions exists as the U^{6+} ion, but in anoxic conditions, this can be reduced to the immobile U^{4+} ion (Tribovillard et al., 2006). Langmuir (1978) argued that the reduction of sulphates to sulphides in anoxic settings results in the inorganic removal of U from the water column. Precipitation is allowed under these conditions, as the U^{4+}ion accumulates along with biogenic material at the sediment-water interface (Lüning & Kolonic, 2003). Previous studies have documented that U forms a close correlation with TOC content in organic rich shales (Renchun, Yan, Sijie, Shuai, & Li, 2015; Schovsbo, 2002).

In short, the U^{4+} ion can be deposited into sediment under reducing conditions, but the process may be increased by the onset of euxinia, where a large input of organic material helps the formation of organometallic complexes via reaction with humic acids (Klinkhammer & Palmer, 1991; McManus, Berelson, Klinkhammer, Hammond, & Holm, 2005).

Using data of the enrichments of Mo and U with respect to TOC in bulk sediments, the oxic, dyoxic, anoxic and euxinic redox conditions can be inferred (Lyons, Reinhard, & Planavsky, 2014; Klinkhammer & Palmer, 1991). Redox sensitive element abundances from the Fraynes Formation exhibit a strong covariance with respect to TOC. This relationship is most prominent in Mo for when TOC was more than 0.5% and less than 4% (Figure 3), indicative of anoxic conditions. A single sample with 8.1% TOC shows strong enrichment in both Mo and U, indicative of euxinic conditions in which both organic and sulphide phases are prominent sinks for Mo and U. These enrichments, with respect to TOC, are consistent with the stratigraphically

younger Mesoproterozoic black shales from the McArthur Basin (i.e., the Velkerri Formation; Cox et al., 2016), which similarly indicate anoxic conditions below 4% TOC and euxinic conditions above ca. 4% TOC (Figure 3). Due to a relatively low sampling resolution of the Fraynes Formation used in this study, the true euxinic threshold for the Limbunya Package can only be assumed to exist between ca. 4% and 8.1% TOC, and a more detailed systematic high-resolution sampling would be necessary to refine the stratigraphic position and timing of such true euxinic conditions.

These relationships between TOC and the proxy-inferred transition from anoxic to euxinic conditions in the basin are not surprising for Proterozoic depositional settings (Cox et al., 2016). The increase of decaying organic matter within the basin can lead to a high oxidant demand in bottom waters, as the remineralisation process starves the system of free O_2 and oxidant (Jenkyns, 2010). The reduction of organic matter can continue by using secondary oxidant sources (Tribovillard et al., 2006) in a predictable order dependent the thermodynamically favourable compounds (NO_3^-, Fe^{3+} then SO_4^{2-}; Kouhasuer, 2009). Because of the relatively low pO_2 environment in the mid-Proterozoic, and the anticipated low levels of nitrate and sulphate in seawater (Fennel et al., 2005; Jenkyns, 2010), the prominent electron acceptors in such setting would be ferric iron. Johnston et al. (2010) argued that in such low pO_2 conditions, once the Fe^{3+} pool is exhausted, any further reduction will result in the onset of euxinia. As a result, the evidence suggests that the transition of anoxic to euxinic conditions during the Fraynes Formation is dependent on the relative input on organic material, and the relative concentration of ferric iron within the basin.

Other examples of deposition under euxinic conditions within the Manbulloo S1 core were not observed, this could be due to limited geochemical resolution resulting in

other euxinic intervals not becoming identified, or that euxinia only existed for a brief period. The latter is consistent with Lyons et al. (2014), who argued that the effect of euxinia on the seawater Mo inventory results in self-limitation, as Mo is an essential micronutrient required for the reduction of nitrogen.

Cerium is a useful as a paleo-redox proxy because it is one of two Rare Earth Elements (REE) that exists in multiple redox states (the other being Europium). While all other REEs are trivalent, Ce^{3+} can be oxidised to Ce^{4+}. As such, the abundance of Ce can be enriched or depleted in seawater and/or marine sediments relative to the neighbouring trivalent lanthanides, depending on the redox state of the water column (Wilde, Quinby-Hunt, & Erdtmann, 1996). The relative enrichment/depletion of Ce is expressed as Ce*, where the concentrations are normalised to shale (PAAS) to remove natural variations in the absolute concentration of REE (Tostevin et al., 2016).

Under persistent and widespread oxic conditions, Ce^{4+} is removed from the seawater by ion (e.g., Mn) hydroxide phases, consequently seawater and authigenic phases (other than iron (oxy)hydrides) precipitated from seawater will show a negative Ce anomaly. In contrast, under persistent and widespread anoxic conditions, Ce anomalies will not develop, as the chemical properties of Ce are similar to La and Pr (Wang, Liu, & Schmitt, 1986). Thus, in redox stratified waters, one can observe both negative and positive Ce anomalies in seawater, due to the remineralisation of iron (oxy)hydroxides as they pass through the redox cline (Elderfield & Greaves, 1981). As a result, the presence of Ce anomalies implies active redox cycling of Ce with the water column (Slack et al., 2007). To determine whether the Ce anomalies are independent of a possible La anomalies, the Ce* was plotted against Pr* to define the ‘true’ Ce anomaly, using the criteria from Bau and Dulski (1996), as shown in Figure 8.

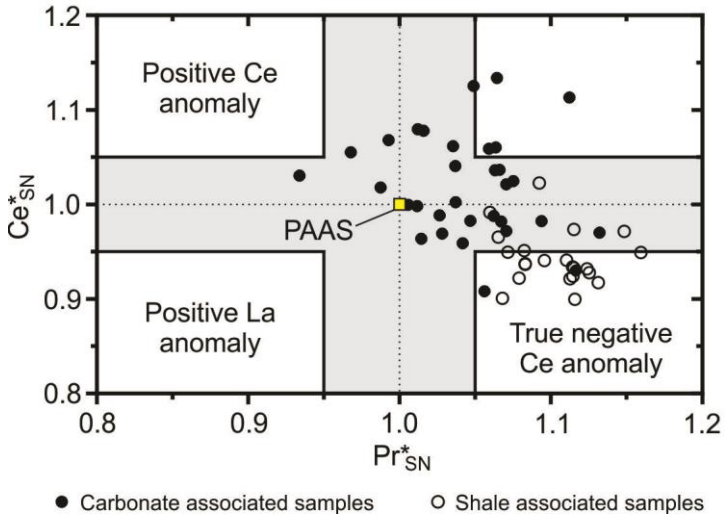

Figure 8: Ce and Pr anomoly cross plot, based on Bau and Dulski (1996). Cerium anomaly calculated as $Ce^*_{SN} = Ce_{SN}/[\sqrt{La_{SN} \times Pr_{SN}}]$, and the Pr anomaly is calculated as $Pr^*_{SN} = Pr_{SN}/[\sqrt{Ce_{SN} \times Nd_{SN}}]$. SN refers to shale normalisation using values for PAAS from Nance amd Taylor (1976).

While most calculated Ce anomalies fall within the values that are indeterminate, many examples exhibit a true negative Ce* signatures that are indicative of oxidative cycling of Ce (Figure 8). These true negative Ce anomalies are almost entirely hosted within the Fraynes Formation, and seemingly represent a local oxidation event within the basin. This does not confer with previous evidence of anoxic to euxinic conditions, and instead the negative Ce* results could be representative of the intersection of the redoxcline relative to the sediment-water interface (i.e., tracing the changes in Ce* of the water column in the McArthur Basin due to the relative changes in the depth of the deposition of Fraynes Formation). German et al. (1991) observed that the Ce* anomalies in the Black Sea water column are not static, but display variation with respect to the depth or position of the redoxcline, with the most negative values occurring at depth of the oxic-anoxic interface (see also Figure 9d).

C-isotope constraints on primary productivity and organic matter burial

Isotopic fractionation of carbon occurs because organisms preferentially uptake light carbon isotopes (^{12}C) by discriminating against ^{13}C during the fixation of CO_2 during photosynthesis. As a result, organic material is systematically enriched in the light isotope of carbon compared to the original pool of C used for photosynthesis (Fry et al., 1991; O'Leary, 1981). The absolute $\delta^{13}C$ value varies depending on different biological carbon fixation mechanisms and the overall composition of the dissolved inorganic carbon (DIC) pool.

Carbon isotope analysis is commonly undertaken on sedimentary carbonates because the $\delta^{13}C$ value of precipitated carbonates very closely approximates the composition of the DIC pool at the water-sediment interface (Halverson, Wade, Hurtgen, & Barovich, 2010). Consequently, the composition of the DIC pool is largely governed by organic carbon burial and water column stratification. For example, complete organic matter remineralisation coupled with complete mixing results in the isotopic composition of the DIC pool becoming unchanged. In contrast, the Black Sea shows a notable $\delta^{13}C$ isotopic trend with the DIC becoming more negative with depth (Fry et al., 1991). This negative trend is due to the remineralisation of the isotopically light organic matter at the water-sediment interface, and the subsequent release of such isotopically light DIC into the water column. The observed $\delta^{13}C$ gradient of the Black Sea exists because of a lack of vertical mixing associated with salinity stratification (Kemp, Testa, Conley, Gilbert, & Hagy, 2009).

For the late Paleoproterozioc and the early Mesoproterozoic, the $\delta^{13}C$ of carbonate precipitated from seawater has a values typically near 0‰ PDB (Strauss, Des Marais, Hayes, & Summons, 1992; Buick, Des Marais, & Knoll, 1995). Such

anticipated 'normal' seawater $\delta^{13}C$ values are observed throughout the upper half of the core (i.e., in dolomites deposited above the Fraynes Formation). In contrast to this, exclusively negative $\delta^{13}C$ values are observed in the lower half of the core, including the Fraynes Formation (Figure 5a). The transition from negative to positive $\delta^{13}C$ values is abrupt, and coincides with the transition from organic rich dolomitic shales (Fraynes Formation) to pure dolomites of the Reward Formation. The $\varepsilon_{Nd(t)}$ trend based on neodymium isotope data showed input in the basin was distinctly crustal and basement derived, based on potential inliers that are used as an example of basement composition for a likely source of clastic sediments (Cox et al., 2016). Only slight variation in the $\varepsilon_{Nd(t)}$ isotope records was noticed, which gives no convincing evidence that the provenance of Nd sources in shales systematically changed throughout the deposition of the Limbunya Package.

Sr-isotope constraints on the basin restriction

Strontium isotopes are used in the reconstruction of paleo-depositional environments because they track relative contributions of old continental material with radiogenic $^{87}Sr/^{86}Sr$ ratios, and unradiogenic hydrothermal Sr sources in the ocean and/or coastal marine system. Due to the long residence time of Sr in the ocean it is considered to be well mixed in open marine systems (Edmond, 1992), consequently, deviations in $^{87}Sr/^{86}Sr$ ratios to radiogenic values are considered indicative of basin restriction (Kuznetsov et al., 2010), in which input of strontium becomes dominated from continental sources.

Based on the observed carbonate-associated $^{87}Sr/^{86}Sr$ trend from the Manbulloo S1 core, a shift to more radiogenic values, and away from values considered to represent

Paleoproterozoic seawater $^{87}Sr/^{86}Sr$ signature (Kuznetsov et al., 2010; Veizer & Compston, 1976), is observed during the deposition of the Fraynes Formation (Figure 5b). This isotopic shift to non-marine and more radiogenic Sr isotope signatures would be consistent with a transient basin restriction (with respect to an open ocean) during the deposition of the Fraynes Formation.

Importantly, the observed changes to more radiogenic $^{87}Sr/^{86}Sr$ values and lower $\delta^{13}C$ values in the Fraynes Formation have also been documented in the correlative Barney Creek Formation from the central part of the McArthur Basin (Giuliano, 2016; LV09001 core, see Figure 1 and 10), which is more than 400 km away from the Manbulloo S1 site. Together, consistent results from the two different paleo-depositional sites recorded would suggest that such purported restrictive event was a basin-wide phenomena, which inhibited the flow and exchange of waters between the coeval global ocean and the Greater McArthur Basin during the deposition of the Fraynes and Barney Creek Formations. Further evidence for such transient basin restriction and a greater influence of continental sources on water chemistry during deposition of the Fraynes Formation is also found in the trace element data, where a higher percentage of continentally derived cations is interpreted, based on the increased concentrations of Al, Rb and K within the carbonate associated samples (Figure 6).

Paleodepositional and redox reconstruction of the Greater McArthur Basin: Comparisons to the present day Black Sea

Previous studies have shown evidence that stratification was present in the late Proterozoic McArthur Basin water column (Johnston et al., 2008), along with abundant organic matter production and preservation (Giuliano, 2016; Summons, Powell, & Boreman, 1988). Accordingly, it can be assumed that the conditions present in the

modern day and redox stratified Black Sea could be in some way analogous to the conditions during the deposition of the Limbunya Package, especially with respect to chemical, redox and salinity stratification. A comparison of selected isotope and redox signatures measured from Manbulloo S1 sedimentary archives (rock samples from drill core) and the modern Black Sea (water samples) is illustrated in Figure 9.

The purported restrictive event that occurred during the deposition of the Fraynes Formation could lead to the deviation away from the coeval $\delta^{13}C$ marine values, but this does not explain why negative values persisted prior to deposition of the Fraynes Formation. Because the $\delta^{13}C$ of precipitated carbonates is believed to closely approximate the C isotope composition of the DIC pool (Halverson et al., 2010), and the $\delta^{13}C$ of the DIC pool in redox stratified basins is expected to systematically decreases with depth (Fry et al., 1991), it can be assumed that the depth of the water column can also control the $\delta^{13}C$ value of precipitated carbonates in the McArthur Basin. The Ce* data fits in with this interpretation, as the values throughout the Fraynes Formation resemble the trend seen at the sulphide interface in the Black Sea (German et al., 1991). In short, the stratigraphic and systematic changes in $\delta^{13}C$ and Ce* trends recorded in the Fraynes Formation and Overlying Reward Dolomite are consistent with the progressive shallowing of the depositional environment (using Black Sea water column as an analogue, see Figure 9). The absolute values from this comparison only conforms to the $\delta^{13}C$ data, as Ce* is mobilised by oxygen, and the oxygen concentration of the atmosphere during the late-Palaeoproterozioic was much less than present day (Gilleaudeau et al., 2016).

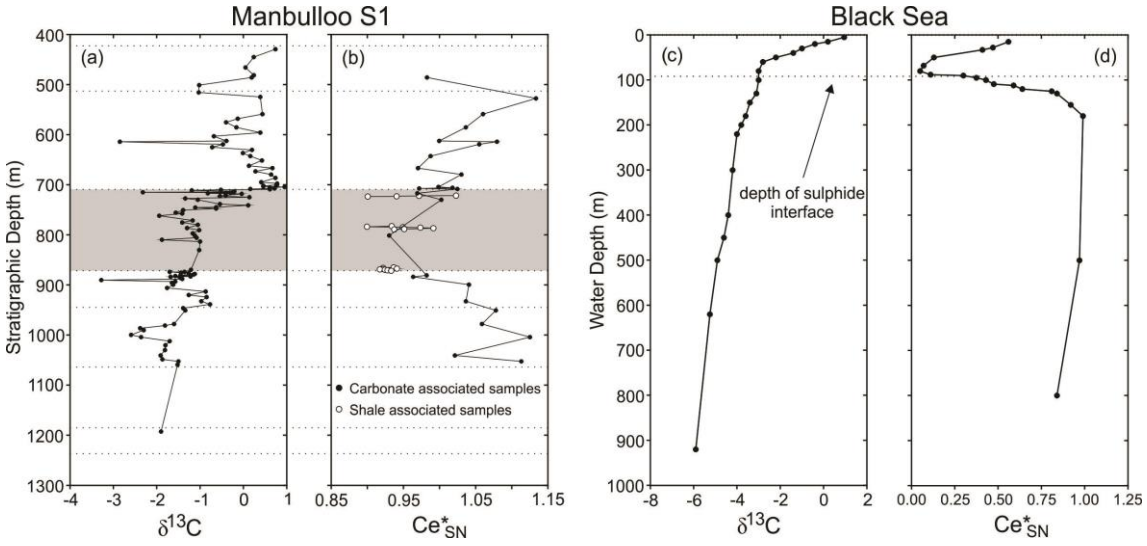

Figure 9: Geochemical comparison of the carbonate-associated $\delta^{13}C$ and Ce* values from the Limbunya Group and the Black Sea. Black Sea data taken from Fry et al. (1991) and German et al. (1991), and relate to water depth. Limbunya Group data is from microdrilled rock samples from the Manbulloo S1 core.

The geochemical and isotope variations observed within the Manbulloo S1 core gives evidence for a significant change in the basin depositional environment throughout the formation of the Limbunya package. From the interpretations made, a major factor of the trends observed within the basin stem from the relationship of distinct layers in a redox stratified water column interacting with the sediment-water interface. The observed trends in the $\delta^{13}C$ and Ce* can be the direct result of a change in water depth (driven by sea level and/or basin subsidence), or they can also be independent of this, and rather reflecting temporal changes in the redox conditions within the water column. In both cases, the chemocline and redox gradient in the water column must have been vertically shifted with respect to the sediment, and the geochemical and isotope indices of the water column conditions interacting at this interface will be integrated into the deposited sediment.

Isotope chemostratigraphy and intra-basin correlations

The comparison between the data sets from the Manbulloo S1 core and the LV09001 core show many similarities and systematic changes for the $\delta^{13}C$ and $^{87}Sr/^{86}Sr$ isotope tracers (Figure 10). The $^{87}Sr/^{86}Sr$ ratio is more continentally influenced during the deposition of both the Fraynes Formation and Barney Creek Formation, suggesting a basin-wide restriction with respect to an open ocean. In contrast, immediately above and below the deposition of these organic-rich dolomitic shales, the $^{87}Sr/^{86}Sr$ ratio of sediments reflects the anticipated mid-Proterozoic paleo-seawater, which indicates an active exchange of water masses between the Greater McArthur Basin and the coeval open ocean, and is therefore unrestricted.

Furthermore, the $\delta^{13}C$ is more negative within the Fraynes and Barney Creek Formations, while trending to more positive values within the overlying Reward Dolomite. The main variance between the data sets from the Manbulloo S1 and LV09001 cores is noted in the Limbunya Package, where $\delta^{13}C$ values recorded in the Campbell Springs Dolomite and Blue Hole Formation are negative, despite the $^{87}Sr/^{86}Sr$ data indicating that the basin had open access to the ocean. The two plausible ways to interpret such variations observed in the studied cores are that there was either (i) a local effect which allowed the two areas to record independent signals (e.g., differences in primary productivity, the isotope composition of the DIC pool), or that (ii) the water depth of carbonate deposition at the Manbulloo S1 site was deeper relative to the LV09001 site, which would translate to more negative $\delta^{13}C$ values of the DIC pool, and thus precipitated carbonates.

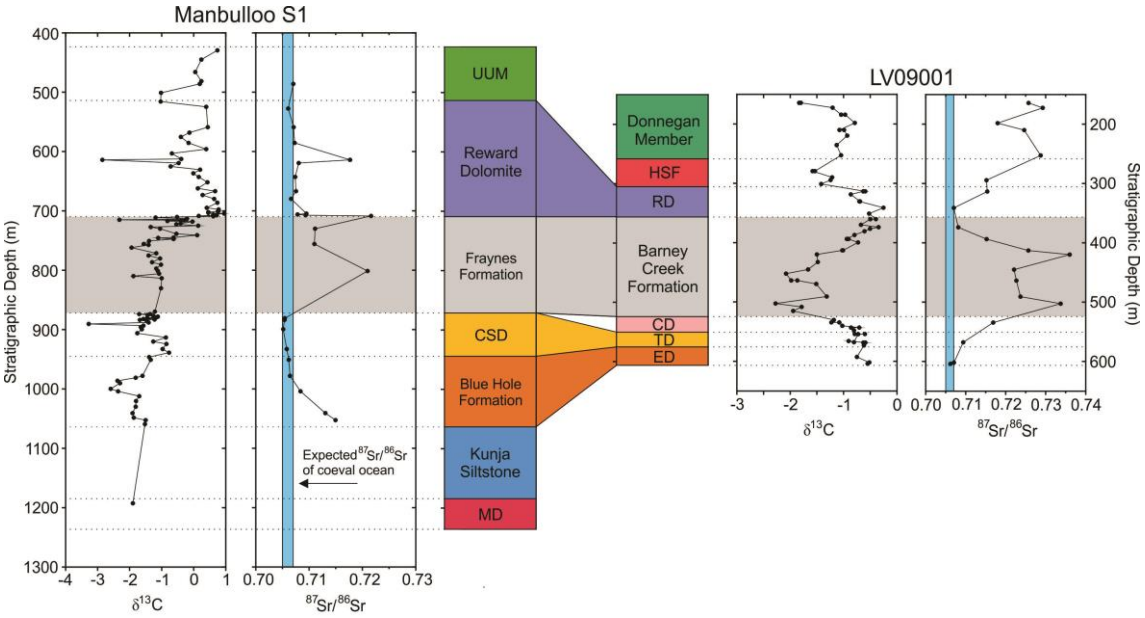

Figure 10: Comparison of key geochemical features from the Manbulloo S1 and LV09001 core. Both cores contain a more radiogenic $^{87}Sr/^{86}Sr$ ratio and a negative $\delta^{13}C$ ratio during the deposition of the Fraynes Formation, and the equivalent Barney Creek Formation. Data from LV09001 taken from Giuliano (2016).

CONCLUSIONS

Using stable and radiogenic isotopes ($\delta^{13}C$, $^{87}Sr/^{86}Sr$ and $^{143}Nd/^{144}Nd$), major and trace elemental concentrations and organic carbon data from the Manbulloo S1 core, the paleo-depositional environment and redox history of the Limbunya Group has been constrained. Results from linking redox-sensitive trace element concentration with TOC showed that deep water anoxia along with transient euxinia were prevalent during the deposition of the Fraynes Formation. These euxinic episodes are proposed to be driven by the input of organic matter, creating oxygen starved bottom waters. Pronounced isotopic signatures ($^{87}Sr/^{86}Sr$ and $\delta^{13}C$) coupled with an increased enrichment of incompatible elements (Al, Rb and K) from samples within the Fraynes Formation (and equivalent Barney Creek Formation) show that during the deposition of the Fraynes Formation, the Greater McArthur Basin was not connected with the global ocean and experienced a basin restriction coupled with redox-stratifacation. In contrast, $^{87}Sr/^{86}Sr$

values from the conformably overlying and underlying dolomitic units are consistent with open ocean conditions, signifying that the Greater McArthur Basin was communicating at some level with an open ocean during these times. Furthermore, comparisons with correlative stratigraphic units from the Manbulloo S1 and LV09001 cores confirmed the existence of basin-wide Sr and C isotope patterns, and thus the potential for future isotopic chemostratigraphy studies for intra-basin correlation purposes in the Greater McArthur Basin.

ACKNOWLEDGMENTS

I would like to thank everyone who has helped me out throughout this year, whether it be academically or personally. Special mentions go to my supervisors, Dr Juraj Farkas and Dr Alan Collins for all the time they gave up, Dr Grant Cox who put in an amazing amount of effort for the project, David Bruce for allowing me to constantly harass him, Bo Yang and Nick Capogreco for great NT times, Dr Alec Walsh for general advice and last but not least, Emma Shaw for drafting and generally keeping me on track all year. Thanks for SANTOS for supplying the funding and allowing great experiences, hopefully this paper is worth it! Finally, thanks to the honours crew for keeping me sane, and I wish you all good luck for the future.

REFERENCES

AHMAD, M., & DUNSTER, J. (2013). Chapter 17: Birrindudu Basin: in Ahmad M and Munson TJ (compilers). *Geology and mineral resources of the Northern Territory. Northern Territory Geological Survey, Special Publication, 5*.

AHMAD, M., DUNSTER, J. N., & MUNSON, T. J. (2013). Chapter 15: McArthur Basin: in Ahmad M and Munson TJ (compilers). *Geology and mineral resources of the Northern Territory. Northern Territory Geological Survey, Special Publication, 5*.

BAILEY, T., MCARTHUR, J., PRINCE, H., & THIRLWALL, M. (2000). Dissolution methods for strontium isotope stratigraphy: whole rock analysis. *Chemical Geology, 167*(3), 313-319.

BANNER, J. L., & HANSON, G. N. (1990). Calculation of simultaneous isotopic and trace element variations during water-rock interaction with applications to carbonate diagenesis. *Geochimica et Cosmochimica Acta, 54*(11), 3123-3137.

BAU, M., & DULSKI, P. (1996). Distribution of yttrium and rare-earth elements in the Penge and Kuruman iron-formations, Transvaal Supergroup, South Africa. *Precambrian Research, 79*(1-2), 37-55.

BETTS, P., ARMIT, R., STEWART, J., AITKEN, A., AILLERES, L., DONCHAK, P., . . . GILES, D. (2016). Australia and nuna. *Geological Society, London, Special Publications, 424*(1), 47-81.

CLOSE, D. [DOROTHY] (2014). *The McArthur Basin: NTGS's approach to a frontier petroleum basin with known base metal prospectivity.* Paper presented at the Annual Geoscience Exploration Seminar (AGES) 2014. Northern Territory Geological Survey.

CLOSE, D. [DAVID], BARUCH, E., COTE, A., ALTMANN, C., MOHINUDEEN, F., RICHARDS, B., & STONIER, S. (2016). *Unconventional gas potential in the Northern Territory, Australia: exploring the Beetaloo Sub Basin.* Paper presented at the AAPG Annual Convention and Exhibition, Calgary.

COLLIER, R. W. (1985). Molybdenum in the northeast Pacific Ocean. *Limnology and Oceanography, 30*(6), 1351-1354.

COX, G. M., JARRETT, A., EDWARDS, D., CROCKFORD, P. W., HALVERSON, G. P., COLLINS, A. S., . . . LI, Z.-X. (2016). Basin redox and primary productivity within the Mesoproterozoic Roper Seaway. *Chemical Geology, 440*, 101-114. doi: 10.1016/j.chemgeo.2016.06.025

CRICK, I., BOREHAM, C., COOK, A., & POWELL, T. (1988). Petroleum geology and geochemistry of Middle Proterozoic McArthur Basin, northern Australia II: assessment of source rock potential. *AAPG Bulletin, 72*(12), 1495-1514.

D. L. SCOTT, D. J., RAWLINGS, R. W. PAGE, C. Z. TAALOWSKI, M. IDNURM, M. J. JACKSON, P. N. SOUTHGATE. (2000). Basement framework and geodynamic evolution of the Palaeoproterozoic superbasins of north-central Australia: an integrated review of geochemical, geochronological and geophysical data. *Australian Journal of Earth Sciences, 47*(3), 341-380. doi: 10.1046/j.1440-0952.2000.00793.x

EDMOND, J. (1992). Himalayan tectonics, weathering processes, and the strontium isotope record in marine limestones. *Science-New York Then Washington-, 258*, 1594-1594.

ELDERFIELD, H., & GREAVES, M. (1981). Negative cerium anomalies in the rare earth element patterns of oceanic ferromanganese nodules. *Earth and Planetary Science Letters, 55*(1), 163-170.

FENNEL, K., FOLLOWS, M., & FALKOWSKI, P. G. (2005). The co-evolution of the nitrogen, carbon and oxygen cycles in the Proterozoic ocean. *American Journal of Science, 305*(6-8), 526-545.

FRY, B., JANNASCH, H. W., MOLYNEAUX, S. J., WIRSEN, C. O., MURAMOTO, J. A., & KING, S. (1991). Stable isotope studies of the carbon, nitrogen and sulfur cycles in the Black Sea and the Cariaco Trench. *Deep Sea Research Part A. Oceanographic Research Papers, 38*, S1003-S1019. doi: 10.1016/s0198-0149(10)80021-4

GERMAN, C. R., HOLLIDAY, B. P., & ELDERFIELD, H. (1991). Redox cycling of rare earth elements in the suboxic zone of the Black Sea. *Geochimica et Cosmochimica Acta, 55*(12), 3553-3558.

GILLEAUDEAU, G. J., FREI, R., KAUFMAN, A., KAH, L., AZMY, K., BARTLEY, J., . . . KNOLL, A. H. (2016). Oxygenation of the mid-Proterozoic atmosphere: clues from chromium isotopes in carbonates.

GIULIANO, W. C. (2016). *Isotope Constraints on Paleo-Depositional Environments and Intra-Basin Correlation in the Proterozoic McArthur Basin, Northern Territory, Australia.* (Honours), University of Adelaide.

HALVERSON, G. P., & HUBERT-THÉOU, L. (2015). Seawater Sr Curve. *Encyclopedia of Scientific Dating Methods*, 733-739.

HALVERSON, G. P., WADE, B. P., HURTGEN, M. T., & BAROVICH, K. M. (2010). Neoproterozoic chemostratigraphy. *Precambrian Research, 182*(4), 337-350. doi: 10.1016/j.precamres.2010.04.007

JENKYNS, H. C. (2010). Geochemistry of oceanic anoxic events. *Geochemistry, Geophysics, Geosystems, 11*(3), n/a-n/a. doi: 10.1029/2009gc002788

JOHNSTON, D. T., FARQUHAR, J., SUMMONS, R. E., SHEN, Y., KAUFMAN, A. J., MASTERSON, A. L., & CANFIELD, D. E. (2008). Sulfur isotope biogeochemistry of the Proterozoic McArthur Basin. *Geochimica et Cosmochimica Acta, 72*(17), 4278-4290.

JOHNSTON, D. T., POULTON, S. W., DEHLER, C., PORTER, S., HUSSON, J., CANFIELD, D. E., & KNOLL, A. H. (2010). An emerging picture of Neoproterozoic ocean chemistry: Insights from the Chuar Group, Grand Canyon, USA. *Earth and Planetary Science Letters, 290*(1), 64-73.

KEMP, W., TESTA, J., CONLEY, D., GILBERT, D., & HAGY, J. (2009). Temporal responses of coastal hypoxia to nutrient loading and physical controls. *Biogeosciences, 6*(12), 2985-3008.

KLINKHAMMER, G., & PALMER, M. (1991). Uranium in the oceans: where it goes and why. *Geochimica et Cosmochimica Acta, 55*(7), 1799-1806.

KONHAUSER, K. O. (2009). *Introduction to geomicrobiology*: John Wiley & Sons.

KUZNETSOV, A. B., MELEZHIK, V. A., GOROKHOV, I. M., MELNIKOV, N. N., KONSTANTINOVA, G. V., KUTYAVIN, E. P., & TURCHENKO, T. L. (2010). Sr isotopic composition of Paleoproterozoic 13C-rich carbonate rocks: The Tulomozero Formation, SE Fennoscandian Shield. *Precambrian Research, 182*(4), 300-312. doi: 10.1016/j.precamres.2010.05.006

LANGMUIR, D. (1978). Uranium solution-mineral equilibria at low temperatures with applications to sedimentary ore deposits. *Geochimica et Cosmochimica Acta, 42*(6), 547-569.

LÜNING, S., & KOLONIC, S. (2003). Uranium spectral gamma-ray response as a proxy for organic richness in black shales: applicability and limitations. *Journal of petroleum geology,* (2), 153-174.

LYONS, T. W., ANBAR, A. D., SEVERMANN, S., SCOTT, C., & GILL, B. C. (2009). Tracking Euxinia in the Ancient Ocean: A Multiproxy Perspective and Proterozoic Case Study. *Annual Review of Earth and Planetary Sciences, 37*(1), 507-534. doi: 10.1146/annurev.earth.36.031207.124233

LYONS, T. W., REINHARD, C. T., & PLANAVSKY, N. J. (2014). The rise of oxygen in Earth/'s early ocean and atmosphere. *Nature, 506*(7488), 307-315.

MCMANUS, J., BERELSON, W. M., KLINKHAMMER, G. P., HAMMOND, D. E., & HOLM, C. (2005). Authigenic uranium: Relationship to oxygen penetration depth and organic carbon rain. *Geochimica et Cosmochimica Acta, 69*(1), 95-108. doi: 10.1016/j.gca.2004.06.023

MUNSON, T. J. (2016). *Sedimentary characterisation and correlation of the Wilton package, greater McArthur Basin.* Paper presented at the Annual Geoscience Exploration Seminar (AGES) 2016. Northern Territory Geological Survey.

NANCE, W. B., & TAYLOR, S. (1976). Rare earth element patterns and crustal evolution—I. Australian post-Archean sedimentary rocks. *Geochimica et Cosmochimica Acta, 40*(12), 1539-1551.

O'LEARY, M. H. (1981). Carbon isotope fractionation in plants. *Phytochemistry, 20*(4), 553-567.

OLAH, G. A., & PRAKASH, G. S. (2017). *Hydrocarbon chemistry*: John Wiley & Sons.

RAWLINGS, D. (1999). Stratigraphic resolution of a multiphase intracratonic basin system: the McArthur Basin, northern Australia. *Australian Journal of Earth Sciences, 46*(5), 703-723.

RENCHUN, H., YAN, W., SIJIE, C., SHUAI, L., & LI, C. (2015). Selection of Logging-based TOC Calculation Methods for Shale Reservoirs: A Case Study of the Jiaoshiba Shale Gas Field in the Sichuan Basin. *Research Institute of Sinopec Exploration Southern Company, Chengdu, Sichuan, 610041*.

REVIE, D. J., & EDGOOSE, C. (2015). *Unlocking potential unconventional petroleum resources in the frontier McArthur Basin, Northern Territory.* Paper presented at the Annual Geoscience Exploration Seminar (AGES) 2015. Record of abstracts'. Northern Territory Geological Survey, Record.

RODRIGUES, S., BLUETT, J., FERGUSON, B. R., GOLDING, S. D., & TITUS, L. (2015). PS Maturation profile at the Glyde Gas Discovery in the Southern McArthur Basin, Australia.

SCHMID, S. (2015). *Sedimentological Review of the Barney Creek Formation in Drillholes LV09001, BJ2, McA5, McArthur Basin*: Northern Territory Geological Survey.

SCHOVSBO, N. H. (2002). Uranium enrichment shorewards in black shales: A case study from the Scandinavian Alum Shale. *Gff, 124*(2), 107-115. doi: 10.1080/11035890201242107

SCOTT, C., & LYONS, T. W. (2012). Contrasting molybdenum cycling and isotopic properties in euxinic versus non-euxinic sediments and sedimentary rocks: Refining the paleoproxies. *Chemical Geology, 324-325*, 19-27. doi: 10.1016/j.chemgeo.2012.05.012

SCOTT, D., RAWLINGS, D., PAGE, R., TARLOWSKI, C., IDNURM, M., JACKSON, M., & SOUTHGATE, P. (2000). Basement framework and geodynamic evolution of the Palaeoproterozoic superbasins of

north-central Australia: An integrated review of geochemical, geochronological and geophysical data. *Australian Journal of Earth Sciences, 47*(3), 341-380.

SHEN, Y., CANFIELD, D. E., & KNOLL, A. H. (2002). Middle Proterozoic ocean chemistry: evidence from the McArthur Basin, northern Australia. *American Journal of Science, 302*(2), 81-109.

SHERROD, L., DUNN, G., PETERSON, G., & KOLBERG, R. (2002). Inorganic carbon analysis by modified pressure-calcimeter method. *Soil Science Society of America Journal, 66*(1), 299-305.

STEPHENSON, M. (2015). *Shale gas and fracking: the science behind the controversy*: Elsevier.

STRAUSS, H., DES MARAIS, D. J., HAYES, J., & SUMMONS, R. E. (1992). Proterozoic organic carbon—its preservation and isotopic record *Early Organic Evolution* (pp. 203-211): Springer.

SUMMONS, R. E., POWELL, T. G., & BOREHAM, C. J. (1988). Petroleum geology and geochemistry of the Middle Proterozoic McArthur Basin, Northern Australia: III. Composition of extractable hydrocarbons. *Geochimica et Cosmochimica Acta, 52*(7), 1747-1763.

TOSTEVIN, R., SHIELDS, G. A., TARBUCK, G. M., HE, T., CLARKSON, M. O., & WOOD, R. A. (2016). Effective use of cerium anomalies as a redox proxy in carbonate-dominated marine settings. *Chemical Geology, 438*, 146-162. doi: 10.1016/j.chemgeo.2016.06.027

TRIBOVILLARD, N., ALGEO, T. J., LYONS, T., & RIBOULLEAU, A. (2006). Trace metals as paleoredox and paleoproductivity proxies: An update. *Chemical Geology, 232*(1-2), 12-32. doi: 10.1016/j.chemgeo.2006.02.012

VEIZER, J., & COMPSTON, W. (1976). 87Sr/86Sr in Precambrian carbonates as an index of crustal evolution. *Geochimica et Cosmochimica Acta, 40*(8), 905-914.

WANG, Y., LIU, Y.-G., & SCHMITT, R. (1986). Rare earth element geochemistry of South Atlantic deep sea sediments: Ce anomaly change at~ 54 My. *Geochimica et Cosmochimica Acta, 50*(7), 1337-1355.

WILDE, P., QUINBY-HUNT, M. S., & ERDTMANN, B.-D. (1996). The whole-rock cerium anomaly: a potential indicator of eustatic sea-level changes in shales of the anoxic facies. *Sedimentary Geology, 101*(1-2), 43-53.

APPENDIX A: FULL DATA SETS

Table 1: Colours representing the separate lithologies of the Limbunya Group, to be used for referencing all future tables.

Colour	Formation name
	Undifferentiated Upper McArthur
	Reward Dolomite
	Fraynes Formation
	Campbell Springs Dolomite
	Blue Hole Formation
	Kunja Siltstone
	Mallabah Dolostone

Table 2: Full data set for the Sm/Nd isotope system

Depth (m)	Nd (ppm)	Sm (ppm)	$^{147}Sm/^{144}Nd$	$^{143}Nd/^{144}Nd$	Stdv for $^{143}Nd/^{144}Nd$	εNd(0)	εNd(t)
467.4	14.578	3.766632	0.15620639	0.511689071	1.69672E-06	-18.5107	-10.0659
500.95	14.481	3.247886	0.135599384	0.511652919	3.00449E-06	-19.2159	-6.42673
699.7	4.5632	1.354315	0.179436819	0.512145455	5.63074E-06	-9.60805	-6.0271
716	17.348	3.47808	0.121212483	0.51157884	2.259E-06	-20.661	-4.84267
734.9	46.574	20.04661	0.260231472	0.511952377	2.11752E-06	-13.3744	-26.8538
819.6	24.464	4.764792	0.117752357	0.511550446	3.3352E-06	-21.2149	-4.66889
873.8	36.874	3.848674	0.063103446	0.510866113	2.27601E-06	-34.5641	-6.5446
1020.2	39.539	4.302478	0.065790035	0.51106144	2.46996E-06	-30.7539	-3.28534
1094.7	38.492	6.575309	0.103277469	0.511356334	2.82143E-06	-25.0014	-5.41746
1233.5	41.041	5.221714	0.076924057	0.51099862	2.96623E-06	-31.9793	-6.86471

Table 3: Full data set of hydrocarbon properties. All samples are from the Fraynes Formation.

Depth (m)	TOC (%)	S1	S2	S3	Tmax	PI
721.49	8.1	0.3	7.03	0.23	449.2325	0.04
722.07	5.6	0.67	2.2	0.07	471.1652	0.23
722.79	1.9	0.19	0.62	0.33	457.5137	0.24
723.36	2.6	0.3	0.74	0.26	447.1505	0.29
782.58	1.4	0.25	0.47	0.29	432.6982	0.35
783.54	1.6	0.27	0.52	0.08	436.5177	0.34
784.65	3.3	0.44	0.97	0.13	442.3781	0.31
785.46	4.6	0.58	1.29	0.09	453.3276	0.31
786.54	4.6	0.59	1.18	0.13	447.0419	0.33
787.31	3.8	0.54	1.17	0.1	469.4154	0.32
788.31	1.6	0.18	0.32	0.17	439.2643	0.35
789.12	1.8	0.2	0.43	0.18	443.0638	0.32
864.7	0.1	0.04	0.09	0.31	447.1067	0.33
865.8	1.3	0.05	0.23	0.03	492.6888	0.17
867.2	0.8	0.03	0.12	0.04	467.701	0.18
868.15	2.2	0.07	0.36	0.05	497.8984	0.16
868.75	1.6	0.05	0.29	0.05	494.3907	0.16
869.58	1.7	0.06	0.3	0.08	501.2026	0.17
870.53	0.3	0.03	0.06	0.23	484.1349	0.34
871.48	2.3	0.06	0.3	0.04	494.8337	0.16

Table 4a: Data set of major and trace elemental concentration for shale associated samples. All samples are from the Fraynes Formation.

	Depth (m)	Fe (%)	SiO2 (%)	Al2O3 (%)	CaO (%)	MgO (%)	MnO (%)	P (%)	S (%)	K2O (%)	Na2O (%)	TiO2 (%)	Cu (%)	Ni (%)	Co (%)
Upper	721.49	0.86	62.38	13.5	0.59	1.49	0.01	0.047	0.138	8.87	0.15	0.42	0.002	0.002	0.003
	722.07	3.87	63.55	10.57	0.52	1.14	0.02	0.071	0.536	6.65	0.17	0.43	0.002	0.003	0.002
	722.79	1.18	38.57	8.95	13.01	8.64	0.05	0.055	0.672	5.58	0.11	0.31	0.002	0.002	0.001
	723.36	1.86	59.89	13.24	2.66	2.41	0.02	0.136	1.446	8.25	0.19	0.55	0.003	0.004	0.003
Middle	782.58	2.23	54.22	11.95	5.73	4.95	0.05	0.12	0.8	6.16	0.23	0.6	0.005	0.002	0.003
	783.54	2.53	62.49	14.77	1.06	2.63	0.02	0.133	1.313	7.4	0.3	0.62	0.004	0.004	0.002
	784.65	2.5	59.1	13.1	2.71	3.22	0.03	0.194	0.903	6.59	0.22	0.56	0.003	0.005	0.002
	785.46	4.72	55.39	13.91	1.39	2.52	0.03	0.118	0.869	6.99	0.21	0.51	0.006	0.005	0.003
	786.54	3	58.66	12.11	2.22	2.8	0.03	0.205	1.193	6.23	0.22	0.57	0.002	0.006	0.002
	787.31	3.79	56.43	13.78	1.87	3.31	0.02	0.158	1.038	6.51	0.24	0.52	0.003	0.007	0.003
	788.31	2.6	60.93	12.73	2.63	3.36	0.02	0.211	1.09	6.24	0.27	0.57	0.003	0.006	0.003
	789.12	2.45	59.05	12.53	3.48	3.68	0.03	0.269	0.993	6.28	0.23	0.52	0.004	0.005	0.003
Lower	864.7	2.51	10.18	2.03	25.94	16.7	0.09	0.005	0.517	0.88	0.01	0.08	0.002	0.002	0.001
	865.8	1.87	60.75	19.09	0.07	1.87	<0.01	0.03	0.787	8.64	0.29	0.66	0.005	0.004	0.003
	867.2	1.9	60.68	19.6	0.07	2.22	0.01	0.027	0.732	8.77	0.3	0.6	0.004	0.006	0.003
	868.15	1.75	61.85	17.9	0.07	1.72	0.01	0.026	0.785	8.52	0.24	0.61	0.007	0.003	0.002
	868.75	1.82	60.9	18.39	0.06	1.92	0.01	0.027	0.946	8.61	0.27	0.65	0.004	0.003	0.003
	869.58	1.66	64.66	13.37	1.47	2.09	0.01	0.027	0.988	7.03	0.17	0.52	0.023	0.003	0.003
	870.53	1.95	28.16	6.05	18.08	12.2	0.09	0.011	0.473	2.88	0.03	0.23	0.004	0.003	0.002
	871.48	1.75	64.02	15.08	0.33	1.58	0.01	0.025	1.129	8.02	0.2	0.55	0.005	0.004	0.005

Table 4b: Data set of major and trace elemental concentration for shale associated samples. All samples are from the Fraynes Formation.

	Depth (m)	Cr (%)	As (%)	Sr (%)	Zr (%)	Ba (%)	V (%)	Cl (%)	Be (ppm)	Bi (ppm)	Mo (ppm)	Rb (ppm)	Tl (ppm)	U (ppm)	Zn (ppm)
Upper	721.49	0.004	0.002	<0.001	0.01	0.048	0.006	0.035	4.5	15.7	101	110	0.5	258	30
	722.07	0.004	0.004	0.006	0.018	0.034	0.003	0.03	3.5	0.3	11	163	1.8	8.8	20
	722.79	0.002	0.002	0.008	0.013	0.026	0.004	0.049	2.5	<0.1	7	109	<0.1	6.3	10
	723.36	0.004	0.004	0.007	0.016	0.042	0.012	0.079	2.5	<0.1	13.5	151	0.2	8.7	14
Middle	782.58	0.004	0.001	0.005	0.011	0.031	0.021	0.065	2.5	0.5	5	392	0.2	5	22
	783.54	0.009	0.002	0.006	0.012	0.035	0.019	0.047	3	0.8	11.5	288	1	5.6	26
	784.65	0.006	0.001	0.006	0.013	0.03	0.012	0.046	2.5	0.2	14.5	182	0.4	11.2	26
	785.46	0.008	0.008	0.008	0.017	0.032	0.015	0.033	2.5	0.2	41	164	1	16.1	24
	786.54	0.007	0.003	0.005	0.012	0.029	0.021	0.038	3	<0.1	28	247	0.7	8	34
	787.31	0.004	0.005	0.005	0.012	0.029	0.024	0.044	3.5	<0.1	27	262	0.8	7.7	30
	788.31	0.006	0.002	0.006	0.013	0.033	0.017	0.068	2.5	0.4	8	245	0.6	6.9	26
	789.12	0.007	0.003	0.005	0.012	0.033	0.021	0.058	2.5	0.3	12.5	193	0.4	7.3	26
Lower	864.7	0.001	0.001	0.005	0.001	0.005	<0.001	0.032	0.5	0.2	2.5	23	<0.1	1.3	6
	865.8	0.008	0.003	0.008	0.012	0.034	0.006	0.055	3.5	0.4	1	269	0.7	2.4	16
	867.2	0.007	0.002	0.006	0.009	0.032	0.005	0.049	4.5	0.4	2	256	0.7	3	16
	868.15	0.006	0.002	0.005	0.008	0.033	0.006	0.05	4	0.5	1	277	0.7	2.4	18
	868.75	0.006	0.003	0.007	0.008	0.031	0.007	0.051	3.5	0.4	1	269	0.7	2.4	14
	869.58	0.005	0.002	0.004	0.02	0.031	0.005	0.036	3.5	0.4	1	162	0.4	2.4	18
	870.53	0.003	0.004	0.004	0.004	0.013	0.001	0.031	1.5	0.1	7	89.8	<0.1	2.6	12
	871.48	0.006	0.004	0.006	0.009	0.027	0.007	0.036	3.5	0.4	3.5	203	0.7	2.5	14

Table 4c: Data set of rare earth elemental concentration for shale associated samples. All samples are from the Fraynes Formation

	Depth (m)	La (ppm)	Ce (ppm)	Pr (ppm)	Nd (ppm)	Sm (ppm)	Eu (ppm)	Gd (ppm)	Tb (ppm)	Dy (ppm)	Y (ppm)	Ho (ppm)	Er (ppm)	Tm (ppm)	Yb (ppm)
Upper	721.49	23.4	55.3	6.65	23.2	4.2	0.7	3.8	0.6	4.05	18.3	0.78	2.4	0.4	2.9
	722.07	36.4	78.1	9.45	30	5.3	0.85	4.2	0.64	3.6	17.8	0.72	2.05	0.25	2
	722.79	23.9	46.1	5.35	17.9	3.3	0.65	3.6	0.54	3.4	16.5	0.68	1.95	0.25	2.35
	723.36	24.3	42.6	4.9	17.1	3.1	0.55	3	0.38	2.5	12.5	0.48	1.4	0.25	1.55
Middle	782.58	33.4	67.8	8.4	29	5.7	1.2	5.6	0.78	4.9	26.4	0.88	2.5	0.3	2.45
	783.54	45.6	84.5	10.3	34.9	5.8	1.05	5	0.64	4.1	20.6	0.76	2.3	0.4	2.4
	784.65	41.5	81.7	9.5	33.3	6.6	1.15	6.6	0.94	5.3	27.8	1	3.05	0.45	2.9
	785.46	47.3	103	12.6	42.9	7.6	1.2	7.4	0.96	6	32	1.24	3.45	0.55	3.8
	786.54	45.4	96.9	11.2	39.9	7.1	1.25	7.2	1.04	6	31.7	1.16	3.4	0.5	3.75
	787.31	38.8	76	8.5	29	5.75	0.9	5.6	0.84	5.3	27.3	1	3.2	0.5	3.35
	788.31	41.5	84.4	10.1	35.7	6.5	1.1	5.8	0.8	5.1	23.5	0.92	2.6	0.3	2.45
	789.12	41.3	85	10.6	39	7.55	1.25	7.2	0.96	5.6	26.9	1.02	2.8	0.3	2.55
Lower	864.7	13.4	27.8	3.5	13	4.95	1.15	5.4	0.74	3.5	14.3	0.6	1.45	0.2	1.1
	865.8	52.8	101	12.1	43.1	6.05	0.9	4.2	0.54	3.45	16.4	0.64	1.85	0.25	1.85
	867.2	52.7	103	12.1	39.9	5.05	0.8	4.2	0.6	3.65	16.6	0.7	1.95	0.3	2
	868.15	45.8	88	10.6	35.7	5.2	0.8	4.2	0.54	3.55	17.7	0.64	1.85	0.25	1.95
	868.75	47.5	91.3	11.1	36.5	4.85	0.75	4.2	0.54	3.45	19.5	0.6	1.85	0.3	1.85
	869.58	40.8	80.1	9.8	33.4	5.6	0.9	4.4	0.62	3.7	16.3	0.64	1.95	0.25	1.95
	870.53	28.3	56	6.85	22.9	5.7	1.05	5.4	0.84	4.35	19.4	0.86	2.3	0.3	2.15
	871.48	44.5	87	10.4	34.6	3.9	0.5	2.4	0.38	2.45	12.4	0.46	1.5	0.2	1.45

Table 5a: Data set of trace and major elemental concentration for carbonate associated samples, including all $^{87}Sr/^{86}Sr$ values. BDL denotes that the elemental concentration was below the detection limit.

Depth (m)	Al (ppm)	P (ppm)	K (ppm)	Cr (ppm)	Mn (ppm)	Fe (ppm)	Cu (ppm)	Rb (ppm)	Sr (ppm)	Mg (ppm)	Ca (ppm)	87/86 Sr	2se for 87/86 Sr
485.75	59.22752	8.902768	22.0764	13.48878	2135.346	2988.451	0.844129	BDL	22.74314	127224.9	173028.4	0.707043	.000012
527.4	126.0765	13.46773	12.76212	0.506999	1725.563	5225.457	0.144587	BDL	25.55389	114692.4	152714.3	0.706081	.000018
558.75	57.58981	4.125094	15.21544	1.239927	2178.407	3397.769	2.311487	BDL	16.1948	101234.2	132527.3	0.707111	.000005
585.35	125.3275	4.249351	22.24953	BDL	1981.788	3422.404	8.998257	BDL	15.86967	101694.8	130117.7	0.707292	.000005
612.4	104.3462	3.88711	6.087747	BDL	2447.061	2519.06	1.744154	BDL	18.63645	726.4434	45388.36	N/A	N/A
613.9	197.612	157.7878	139.1696	BDL	1815.205	741.4657	71.48432	BDL	57.80902	3566.708	261962.9	0.717691	.000007
619.1	98.87622	7.87676	24.16464	0.554041	2418.743	2090.669	1.67279	BDL	15.2008	102233.9	132561.6	0.708052	.000012
642.7	109.3641	6.868489	16.74245	1.94518	1789.037	3710.094	0.908601	BDL	11.25494	104284.8	127719.1	0.707402	.000006
666.7	128.7498	5.25385	9.202534	0.907727	1573.879	2153.672	0.869992	BDL	9.800583	90291.13	122457.8	0.707545	.000018
679.5	71.12716	2.90409	11.01664	BDL	1150.357	2964.029	1.369331	BDL	7.693752	82185.96	115408.9	0.706608	.000008
704.4	506.2067	10.72527	109.2237	1.967851	2512.244	9194.304	1.489229	BDL	18.85588	197604.3	257070.6	0.709495	.000014
705.9	245.2256	7.408066	39.23258	0.648504	1621.029	6301.449	0.449333	BDL	11.16343	109674.4	146268.4	0.707841	.000007
707.2	234.4378	9.583486	45.8839	0.774586	995.6957	4697.358	0.300738	BDL	6.53286	74728.12	101468.1	0.709342	.000006
708.4	900.3545	10.26328	299.606	1.862263	857.8497	4192.005	0.519979	0.388654	7.710029	58451.91	79949.5	0.721634	.000007
729.9	781.6738	17.90583	180.2757	2.678887	666.6174	7582.156	0.696355	0.411079	52.05106	63566.05	204452.5	0.71113	.000004
755.6	326.185	8.499731	90.40946	0.578209	539.0451	2852.955	0.090392	0.129746	20.19736	15542.96	68249.55	0.710993	.000004
801.1	253.152	11.32539	72.93757	0.789583	287.3127	4779.469	BDL	BDL	4.429295	37248.25	59583.28	0.720968	.000011
880.8	195.9813	15.96076	BDL	BDL	1598.547	3950.953	0.3082	BDL	44.7205	116419.7	153811.6	0.705446	.000005
883.7	343.6244	45.00021	5.098613	2.762544	657.4062	6526.649	0.534339	BDL	60.19429	116201.3	161659.8	0.705383	.000004
899.3	338.6968	15.94206	BDL	0.805778	1086.112	4011.715	0.134758	BDL	65.30797	124773.1	179706.9	0.705161	.000003
932.5	577.5197	14.39188	BDL	1.056207	1320.255	3525.676	0.333713	BDL	36.86268	111707.3	142496.9	0.705803	.000006
950.6	415.8493	12.33591	BDL	2.037811	2440.335	4814.622	0.775758	BDL	33.15134	122219.4	158343.1	0.706197	.000004
977.7	345.4435	16.5485	BDL	1.51083	1205.949	5355	0.392686	BDL	33.54708	105506	150333.9	0.706434	.000007
1003.9	701.7281	43.79216	102.0661	3.434225	1300.069	7302.017	0.818516	0.271225	50.43708	109160.3	150388.6	0.708386	.000005
1040.6	542.8998	7.938009	104.2638	1.014857	1467.882	13762.43	0.187887	0.347502	18.2907	92233.63	124781.7	0.713059	.000006
1052.5	947.1958	10.1298	143.8765	1.207105	3549.993	4326.291	1.397722	0.388619	26.0626	117296.5	149740.5	0.714958	.000009

Table 5b: Data set of rare earth elemental concentration for carbonate associated samples.

Depth (m)	La (ppm)	Ce (ppm)	Pr (ppm)	Nd (ppm)	Sm (ppm)	Eu (ppm)	Gd (ppm)	Tb (ppm)	Dy (ppm)	Ho (ppm)	Er (ppm)	Tm (ppm)	Yb (ppm)
485.75	1.486254	3.372975	0.418949	1.534885	0.346888	0.072059	0.456051	0.051847	0.219274	0.039433	0.083373	0.012504	0.064328
527.4	1.035625	3.701346	0.543959	2.28039	0.920247	0.248229	1.711318	0.164419	0.61063	0.098284	0.207121	0.026458	0.155288
558.75	0.318118	1.064493	0.167412	0.752181	0.439363	0.126516	0.879228	0.109446	0.426343	0.065566	0.137762	0.021042	0.106707
585.35	0.357633	1.090676	0.163643	0.702171	0.350123	0.106837	0.855018	0.092593	0.32874	0.047398	0.095239	0.007465	0.068905
612.4	0.434163	1.207883	0.177718	0.835603	0.407658	0.12238	0.88459	0.097382	0.364383	0.04706	0.104754	0.010651	0.06685
613.9	4.985673	14.95972	2.034923	8.733577	2.546105	0.547033	3.113005	0.367788	1.621658	0.247224	0.564721	0.070156	0.377297
619.1	0.349108	0.997725	0.135356	0.633701	0.317389	0.095376	0.612159	0.066308	0.264992	0.03386	0.073389	0.008637	0.042858
642.7	0.350679	0.911228	0.128265	0.517031	0.200027	0.051999	0.39922	0.036125	0.162094	0.025029	0.047842	0.005729	0.030563
666.7	0.381376	0.927284	0.126569	0.435685	0.124046	0.031267	0.204873	0.022471	0.102244	0.017218	0.048373	0.005349	0.032149
679.5	0.468004	1.05484	0.118343	0.491908	0.120217	0.025031	0.166327	0.022211	0.094506	0.015944	0.044109	0.006113	0.030197
704.4	2.114393	4.708905	0.55587	2.072566	0.369818	0.08671	0.458404	0.053668	0.281701	0.053073	0.13994	0.019064	0.116767
705.9	1.602373	3.584988	0.408896	1.545945	0.286958	0.050211	0.258134	0.036708	0.211301	0.036182	0.107644	0.014977	0.089064
707.2	0.954231	2.189162	0.280982	1.017137	0.204234	0.035917	0.205406	0.025179	0.151834	0.026138	0.070015	0.012182	0.059594
708.4	1.689	4.313724	0.554474	1.992407	0.411265	0.075896	0.377165	0.057571	0.343987	0.069651	0.19854	0.0294	0.21125
729.9	20.65125	43.85978	4.897603	16.43221	2.530758	0.367533	1.992276	0.265815	1.364695	0.257969	0.712451	0.091661	0.577234
755.6	5.255767	11.96561	1.261853	4.363922	0.731616	0.121206	0.582226	0.080956	0.451042	0.083601	0.229009	0.032282	0.205872
801.1	2.545604	6.804082	1.110443	4.698645	0.910658	0.176816	0.723181	0.090693	0.447383	0.082784	0.213662	0.025279	0.164629
880.8	0.997863	2.882873	0.456191	1.949969	0.68161	0.145758	0.85742	0.130959	0.637273	0.127953	0.31906	0.056241	0.302802
883.7	1.514818	3.249995	0.396816	1.521848	0.32074	0.076316	0.355998	0.046389	0.212731	0.038168	0.112935	0.01203	0.089381
899.3	1.347967	3.633315	0.477726	1.888473	0.518702	0.136231	0.660242	0.081435	0.371599	0.062322	0.14242	0.016636	0.086794
932.5	1.657662	4.454118	0.588659	2.21195	0.616023	0.139609	0.772499	0.096416	0.517522	0.091078	0.234205	0.031716	0.20134
950.6	0.955764	3.083289	0.45228	2.077312	0.70726	0.173104	0.888444	0.132965	0.745853	0.133395	0.339711	0.04285	0.293879
977.7	2.271837	6.631733	0.912487	3.61706	0.923147	0.202422	1.0799	0.139668	0.648007	0.108921	0.286633	0.030521	0.175603
1003.9	2.210853	8.915629	1.500504	7.418771	2.598731	0.610928	2.988517	0.486666	2.666968	0.451824	1.101138	0.125439	0.71593
1040.6	6.812387	18.1257	2.442803	9.2832	1.778655	0.294199	1.671792	0.230155	1.273648	0.245889	0.619582	0.068424	0.424758
1052.5	3.823145	14.76295	2.430894	10.45565	2.41433	0.457311	2.480946	0.337315	1.77407	0.335594	0.87554	0.109747	0.637809

Table 6: Full data set for the carbon isotope system

Depth (m)	$\delta^{13}C$	stdv	Depth (m)	$\delta^{13}C$	stdv	Depth (m)	$\delta^{13}C$	stdv
429.2	0.74	0.17	710	-0.52	0.03	875.32	-1.44	0.03
444.9	0.24	0.05	711.1	-1.19	0.11	876.6	-1.26	0.02
465.85	0.05	0.08	713	-0.21	0.19	877.9	-1.12	0.08
481.26	0.24	0.04	714.1	-0.23	0.05	878.9	-1.15	0.05
485.75	0.19	0.07	714.8	-2.32	0.45	880.2	-1.45	0.11
500.95	-1.02	0.14	715.5	-0.30	0.07	880.8	-1.22	0.08
515.55	-1.03	0.04	716	-0.40	0.06	881.9	-1.57	0.04
524.45	0.39	0.02	716.95	-0.82	0.11	882.9	-1.22	0.02
558.75	0.44	0.00	717.9	-0.04	0.02	883.7	-1.68	0.04
568	-0.13	0.06	721.1	-0.41	0.14	885.6	-1.46	0.04
575.2	-0.40	0.10	722.37	-0.54	0.23	887.9	-1.41	0.15
585.35	-0.16	0.10	724.7	0.14	0.10	890.2	-3.28	0.04
595.7	0.39	0.05	727.1	-1.34	0.07	893.1	-1.57	0.05
603	-0.68	0.05	729.9	-1.05	0.10	895.6	-1.65	0.05
612.4	-0.39	0.09	738.4	-0.54	0.13	899.3	-1.62	0.20
613.9	-2.85	0.09	740.8	0.11	0.18	905.9	-1.76	0.05
619.1	-0.47	0.07	744.7	-0.63	0.20	913.1	-0.87	0.08
625	-0.72	0.08	745.3	-1.11	0.09	920	-1.26	0.04
630.4	0.20	0.06	747.3	-0.63	0.08	924	-0.85	0.09
636.5	-0.01	0.04	750.4	-1.39	0.07	932.5	-0.97	0.03
642.7	0.16	0.05	755.6	-1.56	0.06	938.6	-0.77	0.09
651.5	0.43	0.02	757.2	-1.41	0.03	946.2	-1.39	0.04
661.85	0.13	0.07	761.7	-1.94	0.26	950.6	-1.34	0.14
666.7	0.67	0.06	771.2	-1.17	0.12	977.7	-1.60	0.10
673.15	0.28	0.02	775.1	-1.41	0.28	980.9	-1.81	0.14
679.5	0.64	0.07	779.9	-1.05	0.12	986.2	-2.38	0.08
686.05	0.74	0.04	786.26	-1.30	0.22	990.13	-2.30	0.12
694.55	0.41	0.05	790.4	-1.02	0.01	999.6	-2.59	0.09
697.3	0.78	0.15	796.97	-1.17	0.02	1003.9	-2.36	0.04
699.7	0.78	0.03	801.1	-1.12	0.08	1012.1	-1.70	0.02
700.5	0.76	0.03	805.7	-1.08	0.01	1020.2	-1.80	0.14
701.8	0.46	0.04	809.73	-1.88	0.14	1029.8	-1.81	0.14
703.2	0.46	0.13	813.25	-1.00	0.14	1040.6	-1.91	0.09
704.4	0.95	0.06	819.6	-1.09	1.09	1048.3	-1.87	0.09
705.9	0.61	0.04	830.17	-1.02	0.02	1052.5	-1.50	0.03
707.2	0.72	0.09	869.58	-1.21	0.41	1059.1	-1.52	0.04
708.4	0.16	0.06	873.8	-1.70	0.10	1192.5	-1.90	0.10
709	0.61	0.17						

APPENDIX B: EXTENDED METHODS

Nd/Sm isotope analysis extended methods, model assumptions and TIMS running modes

Using ion chromatography in polyprep columns containing AG 50W-X8 200-400 mesh resin (separation of rare earth elements from micro-drilled samples), method is as follows:

1: Equilibrate with 6 mL 2 M HCl
2: Load samples in 1 mL 2 M HCl
3: 1 mL 2 M HCl – wash/discard
4: 1 mL 2 M HCl – wash/discard
5: Discard 8 mL 2 M HCl
6: Discard 4 mL 3 M HCl
7: Discard 1 mL 6 M HCl
8: Collect sample in 5 mL 6 M HCl

The subsequent isolation of both Sm and Nd was carried out in quartz glass columns using Eichrom Ln ion exchange resin, with the method as follows:

1: Equilibrate with 4 mL 0.16 M HCl
2: Load samples in 0.5 mL 0.16 M HCl
3: 1 mL 0.16 M HCl – wash/discard
4: 1 mL 0.16 M HCl – wash/discard
5: 13 mL 0.16 M HCl
6: 0.5 mL 0.27 M HCl
7: 3.5 mL 0.27 M HCl – COLLECT Nd fraction
8: 2 mL 0.27 M HCl
9: 3 mL 0.5 M HCl – COLLECT Sm fraction

Table 6: Model assumptions for the Nd isotope system

Nd Model assumptions	Values
Lambda	6.54E-12
143Nd/144Nd CHUR T=0	0.512638 (Goldstein et al., 1984)
147Sm/144Nd CHUR T=0	0.1966 (Goldstein et al., 1984)
143Nd/144Nd DM T=0	0.51315 (Goldstein et al., 1984)
147Sm/144Nd DM T=0	0.2145 (Goldstein et al., 1984)
Earth Age	4.615 Ga

The Nd analysis was carried out on a Finnigan MAT262 TIMS in both static and quadruple cup dynamic measurement modes, with the $^{146}Nd/^{144}Nd$ value normalised to 0.721903. The Sm analysis was carried out on a Finnigan MAT262 TIMS in static measurement mode.

$^{87}Sr/^{86}Sr$ isotope analysis extended methods

The strontium was separated using ion chromatography in polyprep columns containing Eichrom Sr resin SPS, using the following method:

1: Wash resin with 1 reservoir of 3.5 M HNO_3
1: Wash resin with 2 reservoir of DI H_2O
3: Equilibrate resin with 0.5 mL 3.5 M HNO_3
4: Load sample in 0.5 mL 3.5 M HNO_3
5: 2x wash 0.6 mL 3.5 M HNO_3
6: 2x 0.5 DI H_2O – COLLECT Sr fraction

The $^{87}Sr/^{86}Sr$ ratio was measured using a Finnigan MAT262 Thermal Ionisation Mass Spectrometer (TIMS), operating in double collector dynamic measurement mode.

ICP-MS plasma conditions

The plasma conditions for work on the Agilent 8900x QQQ-ICP-MS are as follows: RF power 1550 W, sample depth 8 mm and Ar carrier gas flow rate 1.09 L/min, with a Micro Mist nebuliser and Scott Type spray chamber. The collision cell was run in He mode (4 mL/min He gas flow) and in O reaction mode (30% flow rate). Method from S. Gilbert (personal communication, September 9, 2017)

References

GOLDSTEIN, S., O'NIONS, R., & HAMILTON, P. (1984). A Sm-Nd isotopic study of atmospheric dusts and particulates from major river systems. *Earth and Planetary Science Letters, 70*(2), 221-236.